

# Evolution of a primordial binary black hole due to interaction with cold dark matter and the formation rate of gravitational wave events

Sergey Pilipenko<sup>1</sup>, Maxim Tkachev<sup>1</sup>, and Pavel Ivanov<sup>1\*</sup>

*Astro Space Center, P. N. Lebedev Physical Institute of RAS,  
Profsojuznaya 84/32, Moscow 117997, Russia*

 (Received 27 January 2022; accepted 20 May 2022; published 6 June 2022)

In this paper we consider a problem of formation and evolution of orbital parameters of a binary primordial black hole (PBH) due to gravitational interaction with clustering cold dark matter (CDM). Mass and initial separation have values, which are appropriate for the problem of explanation of the LIGO/Virgo events by coalescing binary PBHs. We consider both radiation dominated and CDM dominated stages of the evolution using numerical and semianalytical means. We show that at the end time of our numerical simulations binary's semimajor axis decreases by approximately one hundred times, while its angular momentum decreases by ten times, in comparison to the standard values, which do not take into account effects associated with CDM clustering. We check that our conclusions are hardly affected by numerical artefacts. We estimate the merger rate of binary PBHs due to emission of gravitational wave at the present time both in the standard case when the effects associated with clustering are neglected and in the case when they are taken into account and show, that these effects could increase the merger rate at least by 6–8 times in comparison to the standard estimate. This, in turn, means, that a mass fraction of PBHs,  $f$ , should be smaller than it was assumed before.

DOI: [10.1103/PhysRevD.105.123504](https://doi.org/10.1103/PhysRevD.105.123504)

## I. INTRODUCTION

Primordial black holes (PBHs) have attracted the attention of many researchers for more than five decades. Depending on their mass they can serve as a candidate for dark matter (see, e.g., Refs. [1–7]), provide seeds for early formation of supermassive black holes (see, e.g., Refs. [8,9]), take an active part in the processes occurring in the early Universe, see, e.g., Refs. [10–12] for a review and further references. The interest to PBHs has been reinvigorated recently after detection of gravitational waves by the Advanced Laser Interferometer Gravitational-Wave Observatory (LIGO) [13–20]. Most of the mergers are associated with binary black holes with masses of order of a few tens of solar masses. It was suggested that the binary black holes involved in these events may be of primordial origin, see, e.g., Refs. [21–24,28].

Therefore, a certain scenario of the formation of binary PBHs must be specified in order to establish the connection between the merger rate needed to explain the LIGO/Virgo events by mergers of binary PBHs and properties of PBH population, most importantly, their typical masses  $M$  and mass fraction of PBHs,  $f$ , of total density of cold dark matter.

Perhaps, the most popular scenario of a kind was put forward by Nakamura *et al.* in 1997 [29] in a different context. It is based on the idea that if a pair of PBHs has an

initial comoving distance between their members,  $d_0$ , smaller than an average comoving distance between PBHs due to statistical fluctuations, it might get bound at times comparable with the time of equipartition between mass densities of cold dark matter (CDM) and radiation,  $t_{\text{eq}}$ . This scenario was developed in the considered context by Sasaki *et al.* [22] and Ali-Haïmoud *et al.* [30] and discussed in some detail below, in Sec. II [31].

The authors cited above neglected the evolution of the bound pairs due to gravitational interactions with the rest of dark matter. On the other hand, from their results it follows that, for typical values of  $M$  and  $f$ , mass of CDM particles enclosed within  $d_0$  of PBH pairs producing the observed merger rate is comparable to  $M$ . In such a situation dynamical gravitational interaction between the pair and CDM could influence orbital parameters of the bound pair, and, in turn, estimates of the merger rate.

Perhaps even more important effect is the formation of halos both around isolated PBHs and, formally, around isolated bound pairs, immersed in an initially spatially uniform distribution of the ordinary CDM particles, see, e.g., Refs. [35,36] and references therein. The effect is more pronounced at relatively late times  $t > t_{\text{eq}}$ , when it may be shown that halo's mass grows approximately proportional to the scale factor,  $s$ , and density distribution of CDM particles has a power law cusp centered at the center of gravity. The presence of such cusps could clearly enhance the interaction between the pair and CDM particles.

\*pbi20@cam.ac.uk

An attempt to answer the question to what extent the interaction between the pair and CDM particles could influence the merger rate was undertaken by Kavanagh *et al.* [37] in 2018. The authors came to the conclusion that this effect plays a minor role in estimates of the merger rates. However, their problem setting was rather unrealistic. They considered, by numerical means, two bound massive particles representing PBHs placed at distances larger than periastron distance of a fiducial Kepler orbit and surrounded by two separate halos of lighter particles with prescribed halo's masses and profiles. The interaction between the pair and the particles occurred mainly at periastron resulting in destruction of the halos and reduction of the pair semimajor axis by a factor of few and an insignificant change of orbital angular momentum. Neither the effects determined by cosmological expansion nor the effect of the formation and growth of the common halo around the pair were taken into account. We are going to show below that taking halo growth into account is crucial in determining the evolution of pair parameters.

In this paper we revisit the problem of interaction between a binary PBH and clustering “ordinary” CDM in an idealized, but self-consistent way. We consider initially unbound pairs of BHs following cosmological expansion at times  $t \ll t_{\text{eq}}$ . These pairs get bound with time, forming a binary PBH [38], and start to interact with the ordinary dark matter. We follow the evolution of the system, containing a PBH pair, dark matter and radiation, well into the matter dominated stage corresponding to times  $t \gg t_{\text{eq}}$ , using numerical and semianalytical means. Typically, our simulations are stopped when the scale factor is ten times larger than its value at the equipartition time. However, when we consider runs with pairs having larger initial separations, we finish our simulations earlier, since we do not find a significant evolution of the quantities of interest at late times in this case. During this evolution, both binary's semimajor axis and its angular momentum get smaller than the values predicted by the purely analytical approaches due to interaction with CDM clustering around the pair. We find these values at the end of calculation and use them to make an estimate of the merger rate, which is then compared with an analytical prediction.

In our numerical work below interaction of the pair with other PBHs is neglected, as well as clustering of radiation and the standard cosmological perturbations of CDM and radiation. Note, however, that we take into account interaction with other PBHs and cosmological perturbations in our estimates of the merger rate using the results of [30]. This is needed because our numerical scheme prohibits very small values of angular momentum that are predicted for the binary PBHs, which may potentially contribute to the event rate. We check that the values of angular momentum obtained as a result of the numerical evolution are proportional to the initial ones, calculate the ratios of these values and use analytical estimates for initial values of

angular momentum to calculate the final values expected for “realistic” binary PBHs. In what follows we assume that the mass fraction of PBHs is much smaller than that of the ordinary CDM,  $f \ll 1$ , and consider the mass densities of radiation and dark matter appropriate for the standard  $\Lambda$ CDM cosmology. We also assume that all PBHs have the same mass  $M$ . In this setting the problem is fully characterized by  $M$  and the initial comoving distance between the members of the pair,  $d_0$ . We set  $M = 50 M_{\odot}$  in all of our numerical runs and consider  $d_0 = 0.5, 0.95, 1.5$  and 2 in units of  $\bar{R} = \sqrt[3]{\frac{3M}{4\pi\rho_{\text{eq}}}}$  (where  $\rho_{\text{eq}}$  is the matter density at the matter-radiation equipartition), noting that our results can be extended to other values of mass by an appropriate redefinition of  $d_0$ .

Although we neglect any perturbations of the system other than those induced by the pair itself, there is an inevitable numerical noise. We check that this noise does not influence significantly our results by performing runs with different numbers of particles representing the ordinary CDM and considering runs with a single PBH with mass  $2M = 100 M_{\odot}$ . Only those results which are stable with respect to a change of the number of particles are taken into account.

We find that the final binary angular momentum gets typically ten times smaller than its initial value, while the semimajor axis typically decreases by  $10^2$  times in comparison with the analytical results. These changes are apparently caused by two effects. At first, a strong decrease of both quantities is observed when the members of the pair approach periastron at the first time. This may be due to expulsion of a significant mass of CDM particles from its vicinity during this time. Second, there is a secular change of these quantities afterwards. We discuss below that it may be due to the effect of binary's “hardening” due to gravitational interaction with CDM particles with sufficiently small angular momenta, which are constantly supplied to the halo, and, then, to the vicinity of binary PBH, from the ambient medium in course of the halo's growth. While the former effect is more significant for the runs with larger values of  $d_0$ , the latter one is more pronounced for the smaller values. We propose a quantitative semianalytical model of the hardening process.

Depending on a value of  $f$ , our estimate of the merger rate, which takes into account these effects gives values  $\sim 6$ – $8$  times larger, than a value, which is obtained neglecting them. This, in turn, means, that in order to satisfy the observational limit on the merger rate, a value of  $f$  should be a few times smaller than the standard estimate. We stress that these results should be treated as a preliminary ones. Since the hardening proceeds until the end of our simulation, it could be effective at later times. This could lead to even larger values of the merger rate. On the other hand, the unaccounted effects of perturbations of orbits of CDM particles could influence our results in the opposite

way due to the presence of other PBHs and cosmological perturbations.

The structure of the paper is as follows. In Sec. II we introduce our basic definitions, relations, and results of the solution of an equations describing dynamics of the pair in the absence of the effects of clustering CDM. Section III is devoted to the numerical simulations, while in Sec. IV we make estimates of the merger rate. We conclude and finally discuss our results in Sec. V.

## II. BASIC DEFINITIONS AND RELATIONS

### A. Notations and conventions

In what follows we neglect the influence of primordial black holes (PBHs) on the overall expansion of the Universe, assuming that it mainly consist of radiation and dustlike cold dark matter (CDM) particles. We are going to consider processes occurring at epochs before and after equipartition time,  $t_{\text{eq}} \approx 23000 \text{ yr}$ , defined by the usual condition that mass densities of matter and radiation are equal to each other at this time, and we denote these mass densities as  $\rho_{\text{eq}}$ . The scale factor,  $s$ , is assumed to be equal to one when  $t = t_{\text{eq}}$ . From the first Friedman equation we easily find a relation between  $t_{\text{eq}}$  and  $\rho_{\text{eq}}$

$$G\rho_{\text{eq}}t_{\text{eq}}^2 = \frac{3\alpha^2}{16\pi}, \quad \alpha = \frac{2}{3}\sqrt{2}(2 - \sqrt{2}) \approx 0.552, \quad (1)$$

where  $G$  is gravitational constant. Also, by integrating this equation we obtain

$$\sqrt{(1+s)}(s-2) + 2 = (2 - \sqrt{2})\tilde{t}, \quad \tilde{t} = t/t_{\text{eq}}, \quad (2)$$

as well as useful relations between  $s$  and its first and second derivatives with respect to the time  $\tilde{t}$

$$\dot{s} = \frac{2}{3}(2 - \sqrt{2}) \left( \frac{\sqrt{1+s}}{s} \right), \quad \ddot{s} = -\frac{4(2 - \sqrt{2})^2}{9} \frac{(1+s)}{s^3}, \quad (3)$$

where dot stands for the derivative with respect to  $\tilde{t}$ . In the asymptotic limits  $\tilde{t} \rightarrow 0$  and  $\tilde{t} \rightarrow \infty$  from (2) it follows that  $s \approx (\frac{4}{3}(2 - \sqrt{2})\tilde{t})^{1/2}$  and  $s \approx ((2 - \sqrt{2})\tilde{t})^{2/3}$ , respectively.

In our analytical and numerical work we formally assume that a mass fraction of primordial black holes is  $f < 1$  and all black holes have the same masses  $M = 50M_{\odot}$ . Our main results can be extended to other values of mass, therefore, we use dimensionless mass  $M_* = \frac{M}{50M_{\odot}}$  in our expressions below as a parameter. A physical distance between two particular black holes is denoted by  $R$ , while the corresponding comoving distance,  $R/s$ , is  $D$ . It is convenient to introduce an average distance  $\bar{R} = \sqrt[3]{\frac{3M}{4\pi\rho_{\text{eq}}}}$  and the associated dynamical time  $t_d = \sqrt{\frac{\bar{R}^3}{GM}}$ . From Eq. (1) we have

$$t_d = \frac{2t_{\text{eq}}}{\alpha} \approx 3.62t_{\text{eq}}. \quad (4)$$

Dimensionless physical and comoving distances are, respectively,  $r = R/\bar{R}$  and  $d = D/\bar{R}$ . It turns out that the evolution of a separated binary black hole depends significantly on initial separation between binary components,  $d_0 = d(\tilde{t} \rightarrow 0)$ . This quantity will be used to characterize different initial conditions for our numerical simulations.

### B. An equation describing the evolution of semimajor axis without the effect of CDM clusterization

When clusterization of CDM is not taken into account, one can use a simple ordinary differential equation to describe the evolution of  $R$ , its time derivative, and, accordingly, binary's semimajor axis  $a = \frac{GM}{|E|}$ , where  $E$  is binary's binding energy per unit of mass [39], see, e.g., Ref. [40]. In what follows we neglect orbital angular momentum of the binary, formally assuming that its eccentricity equals to one, see, e.g., Refs. [22,29,30] for justification of this assumption. In this case the dynamical equation for the evolution of  $R$  has the form

$$\ddot{R} - \frac{\ddot{s}}{s}R = -\frac{2GMt_{\text{eq}}^2}{R^2}, \quad (5)$$

where the second term on the left-hand side (lhs) describes cosmological tidal forces, its explicit form follows from (3), the term on right-hand side (rhs) is the usual Newtonian gravitational force per unit of mass, and we remind the reader that dot stands for differentiation over  $t/t_{\text{eq}}$  [41]. We introduce  $r = R/\bar{R}$ , use the definition of  $\bar{R}$  and Eq. (1) to bring (5) to the form

$$\ddot{r} - \frac{\ddot{s}}{s}r = -\frac{\alpha^2}{2r^2}, \quad (6)$$

which should be solved subject to the condition that  $r \rightarrow s(\tilde{t})d$  when  $\tilde{t} \rightarrow 0$ . Using the definitions of binding energy and semimajor axis as well as (1) we can easily express them in terms of the dimensionless distance  $r$  and its time derivative

$$E = \epsilon \frac{\bar{R}^2}{t_{\text{eq}}}, \quad a = \frac{\alpha^2}{4\epsilon} \bar{R}, \quad \epsilon = \frac{\alpha^2}{2r} - \frac{\dot{r}^2}{2}. \quad (7)$$

In general, Eq. (5) should be solved numerically, and its solutions could be parametrized by values of the initial comoving distance,  $d_0$ . These solutions have the following qualitative behaviour. Initially, at sufficiently small values of  $\tilde{t}$ , the pair is unbound and the distance follows the Hubble expansion,  $r \approx s(\tilde{t})d$ . However, the relative importance of gravitational attraction of the companion black

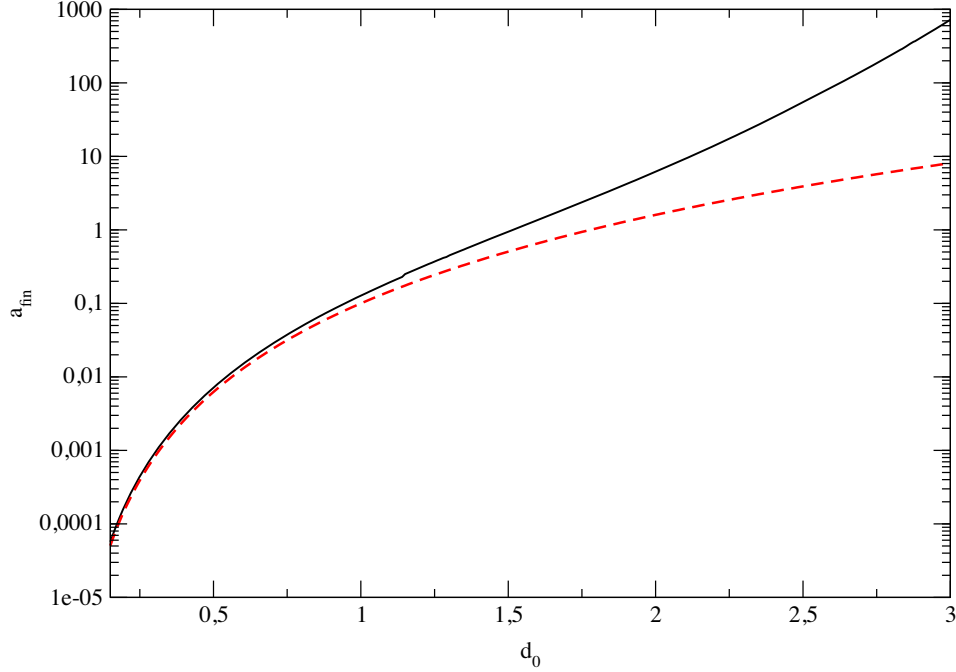


FIG. 1. The dependency of the semimajor axis  $a_{\text{fin}}$  expressed in units of  $\bar{R}$  on  $d_0$ , shown as the solid line as well as its approximate value valid at small  $d_0$  and given by the first expression in (8) given as the dashed line.

hole grows with time, and, at a certain time  $t_{\text{bind}}$  defined by the condition that  $E(t_{\text{bound}}) = 0$ , the pair gets bound, with its binding energy larger than zero. During the following stage the semimajor axis monotonically decreases up to some approximately constant value  $a_{\text{fin}}$ . At later times, in the absence of interaction with accreting dark matter,  $a_{\text{fin}}$  is assumed to be changed only by emission of gravitational waves and we are going to compare our numerical results on the evolution of  $a$  due to interaction with CDM with  $a_{\text{fin}}$ . The stage of a significant decrease of  $a$  terminates when  $r$  becomes formally equal to zero at first time, and we denote this moment of time as  $t_{\text{fin}}$ .

When  $\tilde{t}$  is small it is easy to see that  $\frac{\tilde{x}}{s} \approx \frac{1}{4\tilde{t}}$  on the rhs of (5). In this case (5) is invariant with respect to a linear change of variables  $r \rightarrow \beta r_n$  and  $\tilde{t} \rightarrow \beta r_n$  provided that  $\gamma^2 = \beta^3$ . The remaining freedom in choosing  $\beta$  and  $\gamma$  can be used to make the asymptotic behavior of  $r_n(\tilde{t}_n \rightarrow 0) \propto \tilde{t}_n^{1/2} d_0$  independent of  $d_0$ . It turns out that in this case one has to use  $\beta \propto d_0^4$  and  $\gamma \propto d_0^6$ . After such a choice of  $\beta$  and  $\gamma$  is made, being considered in terms of the new variables  $r_n$  and  $\tilde{t}_n$  both Eq. (5) and the initial condition to it do not depend on any parameters, and, therefore, the solution to this equation is uniquely fixed. The scaling of all quantities characterizing the solution expressed in terms of the old variables, such as  $s_{\text{fin}}$ ,  $s_{\text{bind}}$  and  $a_{\text{fin}}$  with  $d_0$ , should follow from the scaling of  $\beta$  and  $\gamma$ . The scaling of  $a_{\text{fin}}$  expressed in units of  $\bar{R}$  should be the same as the distance  $r$ , and, accordingly,  $a_{\text{fin}}/\bar{R} \propto d_0^4$  while the scalings of  $s_{\text{fin}}$  and  $s_{\text{bind}}$  should be the same as the scaling of the scale factor  $\propto \sqrt{\tilde{t}} \propto d_0^3$ . The coefficients of proportionality in front of these scaling relations can be

chosen by comparing them to the results of a numerical solution of (5). In this way we obtain that

$$a_{\text{fin}} \approx 0.1 d_0^4 \bar{R}, \quad s_{\text{fin}} \approx 0.56 d_0^3, \quad s_{\text{bind}} \approx 0.17 d_0^3 \quad (8)$$

when  $d_0$  is sufficiently small (see, also, e.g., Ref. [30]).

We plot  $a_{\text{fin}}$  as a function of  $d_0$  in Fig. 1 and  $s_{\text{bound}} = s(t = t_{\text{bound}})$  and  $s_{\text{fin}} = s(t = t_{\text{fin}})$  in Fig. 2 together with the corresponding approximate relations (8). One can see from this figure that the relations (8) are indeed quite close to the numerical solutions at  $d_0 < 1$ . Note that at large values of  $d_0$  the effect of dark matter clusterization is very important and must be necessarily taken into account.

### III. NUMERICAL INVESTIGATION OF THE EVOLUTION OF PBH PAIR AND SURROUNDING CDM HALO

#### A. Simulation code and initial conditions

In order to simulate an interaction of PBHs and surrounding dark matter we use a direct summation N-body 4-th order Hermite code `ph4` which is a part of `Amuse` suite [43,44]. This code is MPI-parallel and we made it also OpenMP parallel. Since we simulate systems at times close to the matter-radiation equality, we implemented radiation as a background. Our system also follows Hubble expansion at the beginning. In cosmological N-body codes this is usually implemented by solving particle motion equations in the comoving coordinates and using periodic boundary conditions. Since we are more interested in the behaviour of a gravitationally bound part of the system,



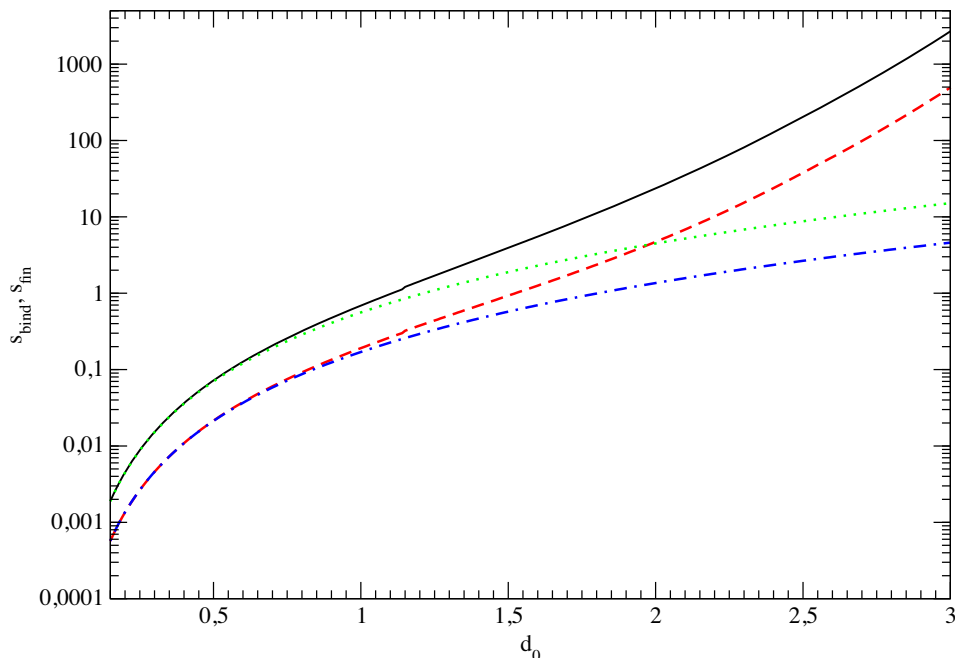


FIG. 2. The dependencies of  $s_{\text{bound}}$  and  $s_{\text{fin}}$  on the dimensionless initial comoving distance  $d_0$  shown as the solid and dashed lines, respectively. Additionally, we show as the dotted and dot-dashed lines  $s_{\text{fin}}$  and  $s_{\text{bound}}$  given by (8).

we use integration in physical coordinates. Periodic boundary conditions will introduce a distortion to the simulation of a spherically symmetric system, so we use vacuum boundary conditions and our system is a sphere with finite radius, large enough to avoid effects of density discontinuity at the sphere boundary on the central part of the system. The sphere is centered at the origin of coordinates. Thus, in order to implement the cosmological background in the simulations, we introduce a radial acceleration, acting on particle at a position  $\mathbf{r}$ :

$$\ddot{\mathbf{r}} = -\frac{\alpha^2}{2} s^{-4} t_{\text{eq}}^{-2} \mathbf{r}. \quad (9)$$

We use a cubic grid for seeding the sphere with DM particles. Particles are assigned velocities according to the Hubble law. In case of a single black hole, it is placed close to the center with a tiny offset  $< 10^{-3}$  of the interparticle distance. If the BH is placed at  $(0, 0, 0)$  exactly, the trajectories of the closest particles pass directly through the BH and the timesteps of the simulation become very tiny, making it impossible to run. We do not take into account the absorption of DM particles by BHs in our simulations.

In case of a pair of BHs, we place them at comoving separation between BHs  $d_0$ , and assign tangential velocities assuming they are at apocenters of pure Keplerian orbits with eccentricity  $e = 0.8$ .

We have made several test runs to check the simulation parameters and a series of production runs, which are summarized in a Table I.

We took caution of choosing a proper value of gravitational softening length  $\epsilon$ . On the one hand, the DM is a collisionless fluid, and it is desirable to have  $\epsilon$  larger than the mean interparticle distance. On the other hand, we are interested in the behavior of a pair of BHs, for which scattering and dynamical friction is important, so  $\epsilon$  should not be too high. Having this in mind, we have conducted tests to check how our results depend on softening. We use the same value of softening length for both DM and BH particles. For a single BH, we have run 5 simulations with 50k particles and the values of  $\epsilon = 4.3 \times 10^{-6}$ ,  $8.5 \times 10^{-5}$ ,  $8.5 \times 10^{-3}$ ,  $2.5 \times 10^{-2}$ , and  $5 \times 10^{-2}$ , respectively. The halo mass growth rate and density profile of these simulations is similar, while the anisotropy and distribution of angular momenta differ significantly. Both anisotropy and angular momentum are larger for simulations with higher  $\epsilon$  when we consider  $\epsilon = 8.5 \times 10^{-5}$ ,  $8.5 \times 10^{-3}$ ,  $2.5 \times 10^{-2}$ , and  $5 \times 10^{-2}$  respectively. The simulation with  $\epsilon = 4.3 \times 10^{-6}$  demonstrates the same distributions of particle angular momentum and anisotropy as the simulation with  $\epsilon = 8.5 \times 10^{-5}$ . As we discuss later on, angular momentum of infalling particles is a crucial parameter determining the evolution of a pair of BHs. From this analysis we conclude that values of  $\epsilon \leq 8.5 \times 10^{-5}$  give stable results which are not affected by softening. For a pair of BHs we have conducted a similar investigation and found that the evolution of the pair semimajor axis is stable for  $\epsilon \leq 8.5 \times 10^{-5}$ . One should note that the mean interparticle distance at the halo center, estimated as  $n^{-1/3}$ , where  $n$  is particle number density, always exceeds  $10^{-3}$  for all our simulations.

TABLE I. List of simulations with their parameters and abbreviations.  $d_0$  is the comoving initial distance between BHs,  $\epsilon$  is the gravitational softening parameter,  $s_{\text{start}}$  and  $s_{\text{end}}$  are scale factors at the beginning and the end of the simulation.  $N$  is the total number of particles, including BHs,  $r_{\text{max}}$  is the comoving radius of the Hubble sphere,  $m_p$  is the particle mass divided by  $2M_*$ .

Simulation	$d_0$	$\epsilon$	$s_{\text{start}}$	$s_{\text{end}}$	$N$	$r_{\text{max}}$	$m_p$
1BH_50k_eps0	0	$4.3 \times 10^{-6}$	0.1	16.2	51 105	3.125	$3 \times 10^{-4}$
1BH_50k_eps1	0	$8.5 \times 10^{-5}$	0.1	3.46	51 105	3.125	$3 \times 10^{-4}$
1BH_50k_eps2	0	$8.5 \times 10^{-3}$	0.1	3.46	51 105	3.125	$3 \times 10^{-4}$
1BH_50k_eps3	0	$2.5 \times 10^{-2}$	0.1	3.46	51 105	3.125	$3 \times 10^{-4}$
1BH_50k_eps4	0	$5 \times 10^{-2}$	0.1	3.46	51 105	3.125	$3 \times 10^{-4}$
1BH_50k_early	0	$4.3 \times 10^{-6}$	0.001	4.15	51 105	3.125	$3 \times 10^{-4}$
1BH_200k	0	$4.3 \times 10^{-6}$	0.1	8.7	203 966	3.125	$7.7 \times 10^{-5}$
2BH_5k_d0.95	0.95	$4.3 \times 10^{-6}$	0.1	8.1	4947	3.125	$3 \times 10^{-3}$
2BH_50k_d0.95	0.95	$4.3 \times 10^{-6}$	0.1	16.2	51 106	3.125	$3 \times 10^{-4}$
2BH_50k_d0.95_eps1	0.95	$8.5 \times 10^{-5}$	0.1	8.1	51 106	3.125	$3 \times 10^{-4}$
2BH_50k_d0.95_eps2	0.95	$1.7 \times 10^{-2}$	0.1	8.1	51 106	3.125	$3 \times 10^{-4}$
2BH_200k_d0.95	0.95	$4.3 \times 10^{-6}$	0.1	10.6	20 3967	3.125	$7.7 \times 10^{-5}$
2BH_50k_d0.7	0.7	$4.3 \times 10^{-6}$	0.001	5.6	51 106	3.125	$3 \times 10^{-4}$
2BH_5k_d0.5	0.5	$4.3 \times 10^{-6}$	0.001	8.1	4947	3.125	$3 \times 10^{-3}$
2BH_50k_d0.5	0.5	$4.3 \times 10^{-6}$	0.001	16.2	51 106	3.125	$3 \times 10^{-4}$
2BH_300k_d0.5_large	0.5	$4.3 \times 10^{-6}$	0.001	7.4	29 9821	3.75	$9 \times 10^{-5}$
2BH_200k_d0.5_high	0.5	$4.3 \times 10^{-6}$	0.001	1.1	20 3967	2.5	$3.9 \times 10^{-5}$
2BH_d0.5_small	0.5	$4.3 \times 10^{-6}$	0.001	8.1	20 674	1.25	$5 \times 10^{-5}$
2BH_200k_d1.5	1.5	$4.3 \times 10^{-6}$	0.1	12.4	20 3967	3.75	$1.3 \times 10^{-4}$
2BH_30k_d2.0	2.0	$4.3 \times 10^{-6}$	0.1	38.2	31 105	5.0	$2 \times 10^{-3}$

Having a set of simulations with identical initial conditions and gravitational softening, but different number of DM particles, we investigate how well our results converge with the change of  $N$ , or particle mass  $m_p$ . As seen from Table I, our simulations of a pair with  $d_0 = 0.5$  cover almost 2 orders of magnitude in the particle mass,  $m_p$ .

### B. Properties of halos, formed around single or double BHs

It is well known that in a homogeneous expanding Universe a halo is formed around a single point mass (see, e.g., Gott 1975 [45] and Gunn 1977 [46]). The halo boundary can be characterized by a turn around radius: at this radius a shell of matter turns around its radial velocity from Hubble expansion to infall. As has been shown in [47], the radius and mass of the halo grow with time as:

$$r_{\text{ta}} \propto s^{4/3}, \quad (10)$$

$$M_{\text{ta}} \propto s. \quad (11)$$

We check that our simulations reproduce equations (10) and (11). At the same time we measure halo density profile from our numerical results. To do this, we construct a set of spherical shells centered at the black hole (or at the mass center of the pair, in the case of 2 BHs), each shell containing the same amount of particles  $N_{\text{shell}} = 25$ .

The turn around shell is the furthest shell from the center which has mean radial velocity less than zero. The turn around radius is a radius at which the linearly interpolated mean shell velocity between the turn around shell and the next shell with positive radial velocity equals to zero. The turn around mass is the mass of all particles, except the black hole(s) inside the turn around radius.

In Fig. 3 we show the evolution of  $r_{\text{ta}}$  and  $M_{\text{ta}}$  in several simulations. It is clearly seen that in simulations with a single BH the evolution of these characteristics very well reproduces the Eqs. (10) and (11). Simulations with a pair also show a perfect match until some specific time which is close to the first pericenter passage of the pair. This passage happens at  $s = 1.15$  for simulations with  $d_0 = 0.95$  and at  $s = 0.075$  for simulations with  $d_0 = 0.5$ . After that time, the halo radius becomes somewhat smaller, while the mass drops significantly. The turn around mass evolution of a halo around a pair of black holes is close to  $M_{\text{ta}} \propto s^{3/4}$  at late times. This demonstrates that the pair throws away a significant amount of matter.

Another test of simulations is the density profile of dark matter halos. Theory predicts the formation of a power law profile  $\rho \propto r^{-9/4}$  [47]. In Fig. 4 we demonstrate how our simulated halos follow this predicted law [48]. It is seen that there is a good agreement, but the profile for a single black hole is flattening to  $\rho \propto r^{-1.5}$  at  $r < 0.1$ . For the pair of black holes this flattening is more pronounced, and also the whole profile has smaller values of density

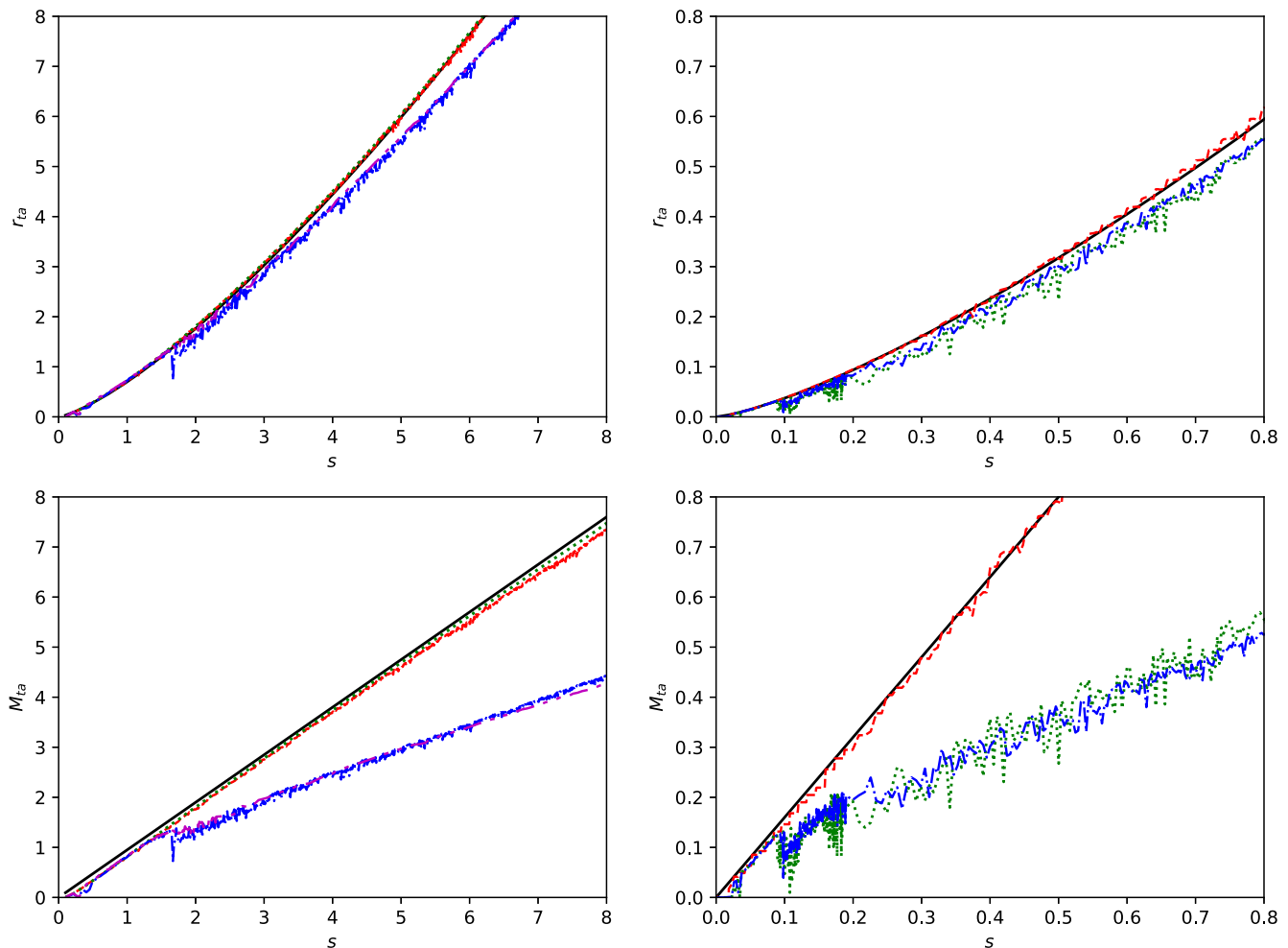


FIG. 3. Left top and left bottom: evolution of the turn around radius and turn around mass in theory,  $r_{\text{ta}} \propto s^{3/4}$ ,  $M_{\text{ta}} \propto s$  (solid lines) and in simulations of single BH 1BH\_50k\_eps0 (dashed lines), 1BH\_200k (dotted lines), and the pairs with  $d_0 = 0.95$ , 2BH\_50k\_d0.95 (dot-dashed lines) and 2BH\_200k\_d0.95 (dot-dot-dashed lines). Right top and right bottom: the evolution of the turn around radius and turn around mass in theory (solid lines) and in simulations of the single BH 1BH\_50k\_early (dashed line) and the pairs with  $d_0 = 0.5$ , 2BH\_50k\_d0.5 (dotted line), 2BH\_300k\_d0.5\_large (dot-dashed line).

than the one corresponding to a single black hole at  $r \lesssim 2$ , which is of the order of the radius of influence of the binary. The effect of flattening of the density profile is clearly determined by domination of gravitational field of the black hole or the binary at small distances. The evolution of halo mass and the dark matter profiles show a remarkable stability with the change of the numerical resolution, i.e., the particle mass  $m_p$  over almost two orders of magnitude.

For the pairs of BHs with a large initial distances,  $d_0 = 1.5$  and  $d_0 = 2$ , there is some notable differences in halo evolution. The two halos around each BH grow in isolation for a long period of time, gaining mass much larger than the mass of BHs they host. After these two halos merge, the resulting single halo shows growth of mass and radius quite similar with the case of a single BH and it is well approximated as  $M_{\text{ta}} \propto s^{0.9}$ , see Fig. 5. However, the halo itself becomes severely anisotropic. We demonstrate it

by measuring the major to minor axis ratio of a reduced gyration tensor, defined as:

$$G_{ij} = \frac{1}{N} \sum_{k=1}^N \frac{x_i^k x_j^k}{r^k r^k}, \quad (12)$$

where  $x_i^k$  is  $i$ th coordinate of  $k$ th particle. We compute  $G_{ij}$  for all particles with  $r < r_{\text{ta}}$ , excluding the BH particles, then we find eigenvalues of  $G_{ij}$ . The axis ratio is defined as the square root of the ratio of maximal and minimal eigenvalues of  $G_{ij}$ . In Fig. 5 we subtract 1 from this axis ratio, i.e., value of 0 corresponds to a spherically symmetric distribution. The halos around BH pairs that have merged earlier are much more spherical, as seen from the evolution of the  $G_{ij}$  axis ratio in 2BH\_50k\_d0.95 simulation in Fig. 5. But the halo around a pair with  $d_0 = 0.95$  is less spherical than a halo around a single BH at times  $s < 5$ .

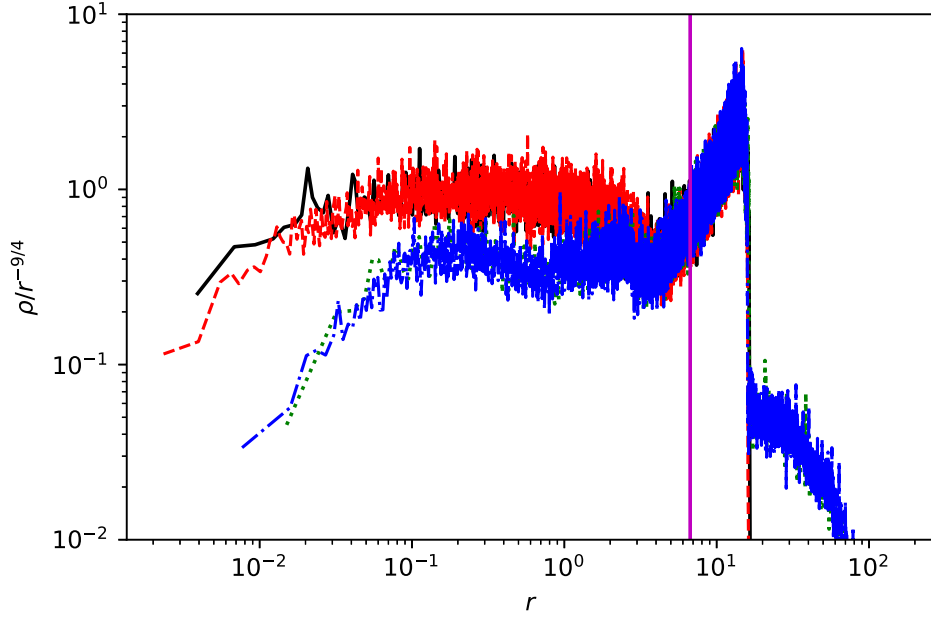


FIG. 4. Dark matter density profiles of halos multiplied by  $r^{9/4}$  at  $s = 5.6$  for simulations: 1BH\_50k\_eps0 (solid line), 1BH\_200k (dashed line), 2BH\_50k\_d0.95 (dotted line) and 2BH\_200k\_d0.95 (dot-dashed line). Vertical black line indicates mean turn around radius of halos in these simulations at  $s = 5.6$ .

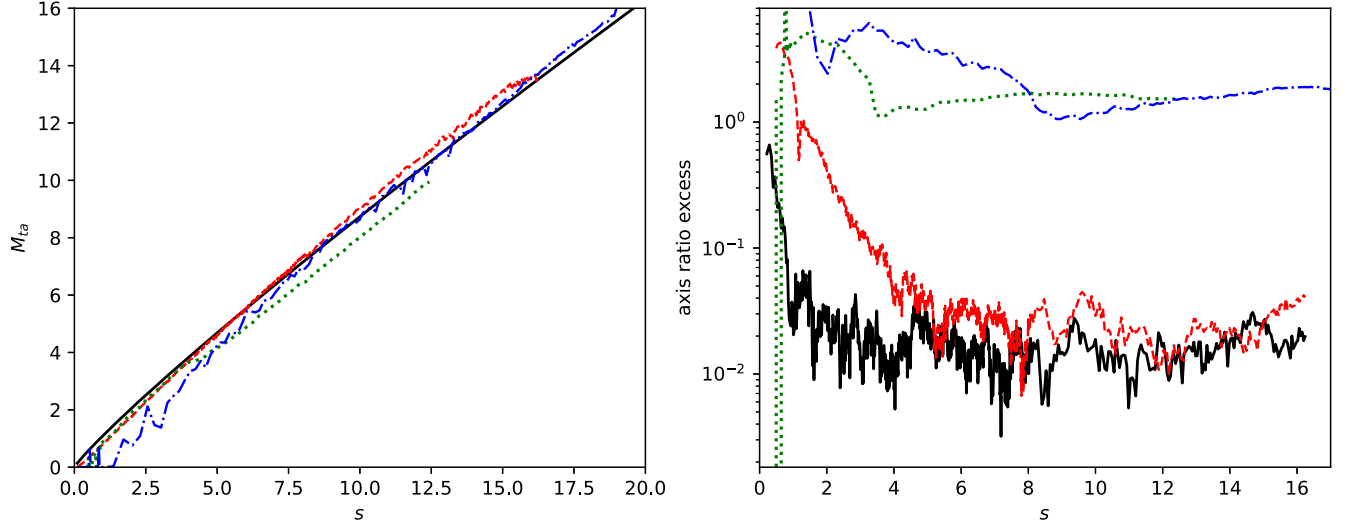


FIG. 5. Evolution of accreted DM halos at late times. Left panel: mass of a halo inside a turn around radius, the approximation  $M_{\text{ta}} \propto s^{0.9}$  (black solid line) and simulation results for 1 BH (1BH\_50k\_eps0, dashed line), and 2 BHs with  $d_0 = 1.5$  (2BH\_85k\_d1.5, dotted line), and  $d_0 = 2$  (2BH\_30k\_d2, dot-dashed line). Right panel: gyration tensor axis ratio excess at turn around radius for simulations with a single BH (1BH\_50k\_eps0, solid line), and for BH pairs with  $d_0 = 0.95$  (2BH\_50k\_d0.95, dashed line),  $d_0 = 1.5$  (2BH\_200k\_d1.5, dotted line), and  $d_0 = 2.0$  (2BH\_30k\_d2, dot-dashed line).

### C. Evolution of a BH pair

We characterize the pair of BHs at every simulation snapshot by two main parameters: the semimajor axis of the orbit  $\tilde{a} = a/\bar{R}$ , where  $a$  is defined in (7) and the dimensionless angular momentum  $l$ , which is computed as

$$l = v_t r, \quad (13)$$

where  $v_t$  is the relative tangential velocity of BHs (measured in units of  $\bar{R}/t_{\text{eq}}$ ).

The results are shown in Fig. 6. The top row demonstrates the numerical convergence over almost two orders of magnitude in test particle mass in case of simulations with  $d_0 = 0.5$ . All simulations with the total number of particles from  $5 \times 10^3$  to  $3 \times 10^5$  show a steady decrease of



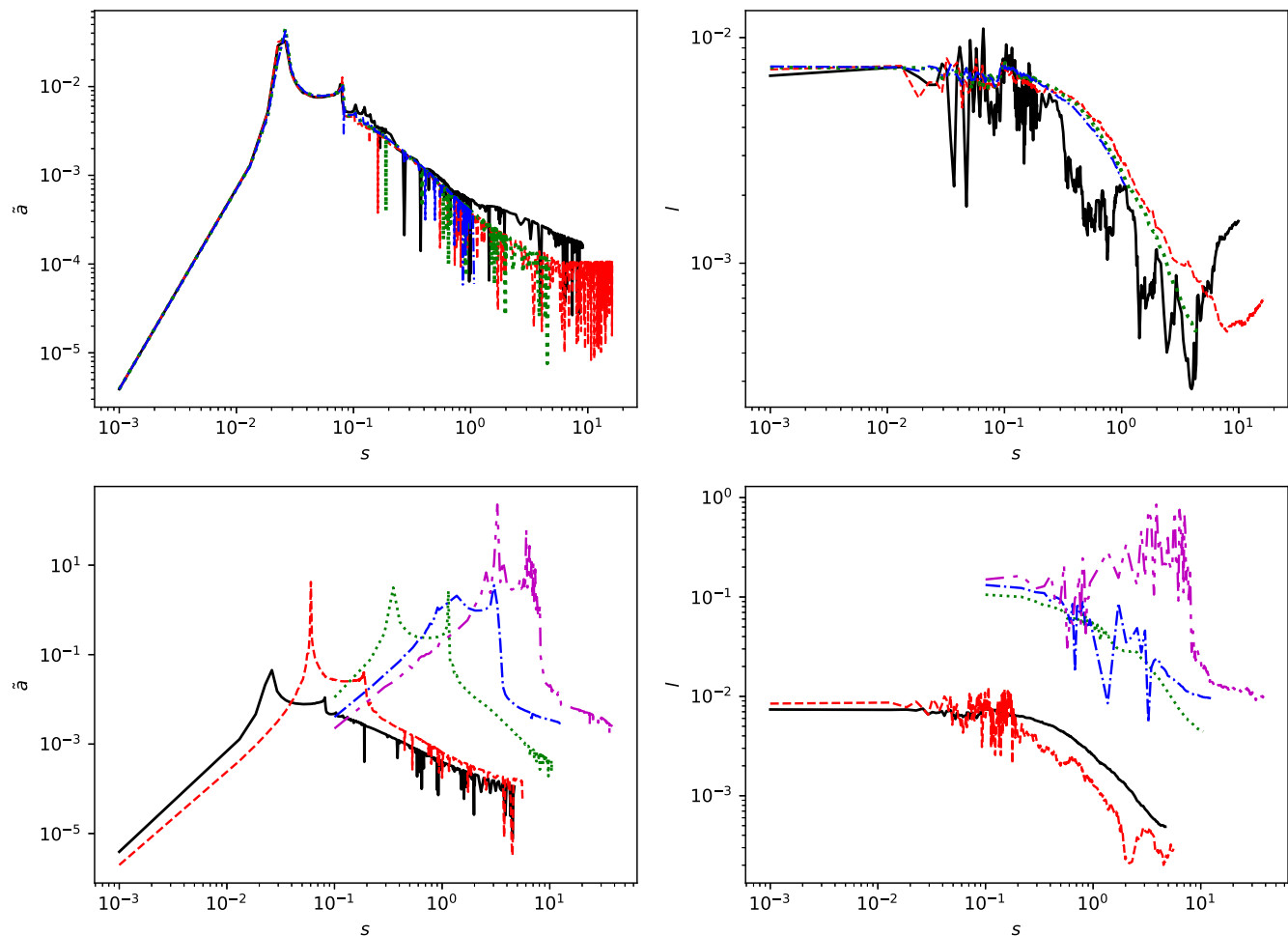


FIG. 6. Top row: convergence of the evolution of dimensionless semimajor axis (left panel) and dimensionless angular momentum (right panel) in simulations with  $d_0 = 0.5$  and  $m_p = 3 \times 10^{-3}$  (solid line),  $m_p = 3 \times 10^{-4}$  (dashed line),  $m_p = 9 \times 10^{-5}$  (dotted line) and  $m_p = 3.9 \times 10^{-5}$  (dot-dashed line). Bottom row left panel: evolution of a semimajor axis of a BH pair in simulations with increasing initial comoving distance  $d_0 = 0.5$  (solid line),  $d_0 = 0.7$  (dashed line),  $d_0 = 0.95$  (dotted line),  $d_0 = 1.5$  (dot-dashed line),  $d_0 = 2$  (dot-dot-dashed line). Bottom right panel: evolution of the dimensionless angular momentum  $l$ . The meaning of line styles and colors is the same as in the left panel.

$\tilde{a}$  after the first passage of pericenter, which happens at  $s \approx 0.08$ . Note that this value is very close to the corresponding value  $s_{\text{fin}}$  obtained from the solution of Eq. (6), see Fig. 2. One should note that due to the decrease of  $\tilde{a}$  with time, at some moment there is less than 1 DM particle between the BHs which affects the pair evolution. For the lowest resolution simulation with  $m_p = 3 \times 10^{-3}$  this happens at  $s = 0.2$ , while for simulations with  $m_p = 3 \times 10^{-4}$  and  $m_p = 9 \times 10^{-5}$  this happens at  $s = 1$  and  $s = 2$ , respectively. Our highest resolution simulation with  $m_p = 3.9 \times 10^{-5}$  is stopped before the regime with less than 1 particle between BHs is reached.

In the bottom left panel of Fig. 6 it is seen that simulations with  $d_0 < 1.5$  show a steady decrease of  $\tilde{a}$  after the first pericenter passage. Simulations with  $d_0 \geq 1.5$  show a rapid drop of  $\tilde{a}$  at the pericenter passage, determined by the merging of two massive halos.

The evolution of the dimensionless angular momentum,  $l$ , in Fig. 6 shows two sets of lines with different initial  $l$ . One set corresponds to simulations which start at  $s_{\text{start}} = 0.001$  and another one corresponds to  $s_{\text{start}} = 0.1$ . This is caused by the preparation of the initial conditions with fixed eccentricity described in Sec. III A. Our results show an approximately tenfold drop of angular momentum during the evolution of the system.

At a first glance our numerical results for the evolution of  $\tilde{a}$  and  $l$  are at odds with the results of [37]. To investigate the cause of the difference, we first run with our code a simulation with the initial conditions from [37], which has the PBH mass  $30 M_\odot$ , the initial semimajor axis  $a_i = 0.01$  pc and eccentricity  $e_i = 0.995$ . These initial conditions have only  $6.2 M_\odot$  mass in the dark matter, which is about 1/10 of the binary mass. We obtain results in a fine agreement with that shown in [37], so the difference with

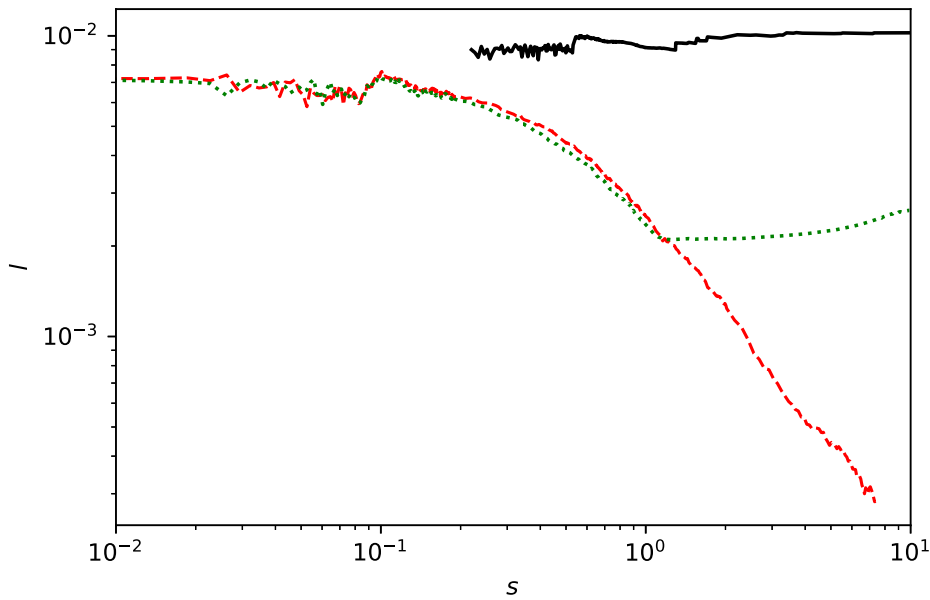


FIG. 7. Evolution of the angular momentum in the simulation from the initial conditions from [37] without cosmological expansion and DM accretion (solid line), in our simulation 2BH\_300k\_d0.5\_large with DM accretion during the full run (dashed line), and in a simulation where the accretion stops due to a smaller size of the Hubble sphere, 2BH\_d0.5\_small (dotted line).

our simulations is not due to the fact that we use a different N-body code. We also run a simulation with the same initial conditions, but with the additional force caused by the radiation background. This gives almost no effect on the evolution of the binary.

Next we check the influence of accretion of DM particles from the Hubble flow. In simulations of [37] there is no such accretion, but according to a simple estimate, the halo around a binary should grow by ten times during the time period shown in Fig. 6 of [37]. We run a test simulation with a Hubble sphere filled by DM particles, as described in Sec. III A, but the sphere radius is artificially chosen small enough to end the accretion in the middle of the simulation (this simulation is labeled as 2BH\_d0.5\_small in Table I). We show in Fig. 7 that when the accretion stops, the angular momentum stops decreasing. The same happens for the semimajor axis. So, we conclude that the accretion of DM particles is the main factor responsible for the late evolution of the PBH pair, after the formation of the common halo. The infalling DM particles have near radial trajectories and thus persistently refill loss cone of the binary, see also the following Section.

#### D. A semianalytic treatment of the late time evolution of semimajor axis and angular momentum

We can see from Fig. 6 when  $d < 0.95$  both semimajor axis and angular momentum experience a steady decrease. As discussed above, the most likely explanation for this behavior is due to “hardening” of the binary due to its interaction with CDM particles having their periastron distances,  $r_p$ , order of or smaller than binary’s semimajor

axis  $a$ . As discussed in, e.g., [49], the contribution of a given particle to the evolution of both quantities is determined by the ratio  $r_p/a$  (or, alternatively, the ratio of particle specific angular momentum to that of the binary), and only the particles with  $r_p/a \sim 1$  can influence it significantly. In principle, the origin of particle’s angular momentum could be due to the tidal torque exerted by the binary on the particles. However, we checked that a value of angular momentum expected from this effect is too small to explain what is observed in simulations. A relatively large value of the angular momentum may be explained by torques acting on the particles from the side of nonspherical part of density distribution of the halos related to the observed halo’s anisotropy. The anisotropy itself may be originated from the action of the radial orbit instability (see, e.g., Ref. [50]) with initial perturbations provided by the action of binary’s quadrupole gravitation field. In this picture the smaller is  $d_0$  the smaller would be the anisotropy and this is indeed observed in the simulations. An analytical calculation of the corresponding distribution of angular momentum is a non-trivial problem, which is left for a future work. In this paper we use an average value of  $r_p$ ,  $\bar{r}_p$ , evaluated numerically at the “influence radius” determined by the condition that halo’s mass inside this radius is equal to that of the binary. We show the dependency of  $\bar{r}_p$  on  $s$  in Fig. 8, for the case  $d_0 = 0.95$ .

Sesana *et al.* [49] showed numerically that, a contribution of a particle with a given value of  $r_p$  to the hardening rate of semimajor axis is determined by a function  $C(x)$  of  $x = \sqrt{r_p/a}$ , while the same contribution to the evolution of angular momentum is given by a similar

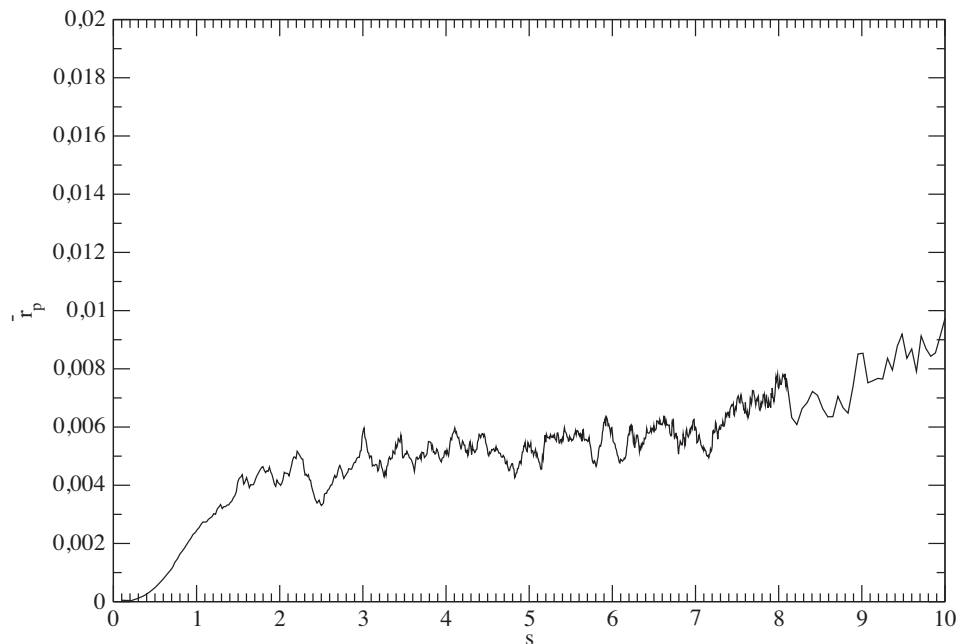


FIG. 8. The dependency of the average periastron radius  $\bar{r}_p$  on  $s$ , taken from the simulation *2BH\_200k\_d0.95*.

function  $B(x)$ . We used their numerical results presented in their Figs 1 and 2, for an equal mass binary with eccentricity  $e = 0.9$  and fitted  $C(x)$  by a simple function,  $C(x) = 2.647(1 + x^2)^{-2}$ , which is in a quite good agreement with the numerical curve.  $B(x)$  is a nonmonotonic function of  $x$ , and, a simple fit of it does not appear to be possible. However, for our purposes we only need to know the integral  $I(x) = \int_0^x dy y B(y)$ , which can be fitted as  $I(x) = 2.86(1 - \frac{1}{(1+x^2)^{3/5}})$  remarkably well.

When  $C(x)$  and  $B(x)$  are known, it follows from the discussion in Sesana *et al.* [49] the time evolution of  $a$  and  $L$  are given by the simple expressions

$$\frac{\dot{a}}{a} = - \int_0^\infty C(x) dP_{r_p} \frac{\dot{M}}{M}, \quad \frac{\dot{L}}{L} = - \int_0^\infty B(x) dP_{r_p} \frac{\dot{M}}{2M}, \quad (14)$$

where  $P_{r_p}(r_p)$  is a probability of finding the periastron radius with a value smaller than  $r_p$ . We model the corresponding probability density as a step function,  $dP_{r_p}(r_p)/dr_p = \frac{1}{2\bar{r}_p} \Theta(r_2 - 2\bar{r}_p)$ , where the factor  $\frac{1}{2\bar{r}_p}$  in the front of the step function  $\Theta(x)$  is chosen in such a way that the average value of  $r_p$  coincides with  $\bar{r}_p$ .  $\dot{M}$  in (14) is the mass flow through the sphere of influence of the pair (i.e., a sphere centered at the center of mass of the binary with the radius equal to the influence radius,  $r_{\text{inf}} \approx 2$ , see the discussion above). We assume that it is approximately the same as the mass flow through the turn around radius,  $\dot{M} \approx M \frac{ds}{dt}$ .

Combining all ingredients discussed above together, we can write down two evolution equations for  $a$  and  $L$ :

$$\frac{1}{a} \frac{da}{ds} = -1.32 \frac{a}{\bar{r}_p} \left( 1 - \frac{1}{1 + \frac{2\bar{r}_p}{a}} \right),$$

$$\frac{1}{L} \frac{dL}{ds} = -1.43 \frac{a}{\bar{r}_p} \left( 1 - \frac{1}{(1 + (\frac{2\bar{r}_p}{a})^3)^{3/5}} \right). \quad (15)$$

As an initial condition we use values  $a_{\text{fin}}$  and  $s_{\text{fin}}$  obtained from the solution of Eq. (6),  $s_{\text{fin}} \approx 0.6$  and  $a_{\text{fin}}(s_{\text{fin}}) \approx 0.1$ . Results of the solution of Eqs. (15) are shown in Figs. 9 and 10. One can show from these figures that, indeed, at sufficiently large values of  $s$  the fully numerical results are quite close to the solutions of (15).

#### IV. ASTROPHYSICAL IMPLICATIONS

In order to see to what extent the additional evolution of semimajor axis and angular momentum due to dynamic influence of CDM accretion would influence the results concerning the possibility of explaining the LIGO events by PBHs, we need to estimate the formation rate of gravitational wave events,  $R$  (or, the merger rate), both, for the case when the effects of CDM clustering are absent and in the case when they are present. In the former case we closely follow Ali-Haïmoud, Kovetz and Kamionkowski 2017 [30] (hereafter, AKK), while in the latter case we use the numerical results obtained above. For the comparison with observations we are going to consider only  $M_* = 1$ , and assume that when  $M_* \sim 1$  observations constraint the

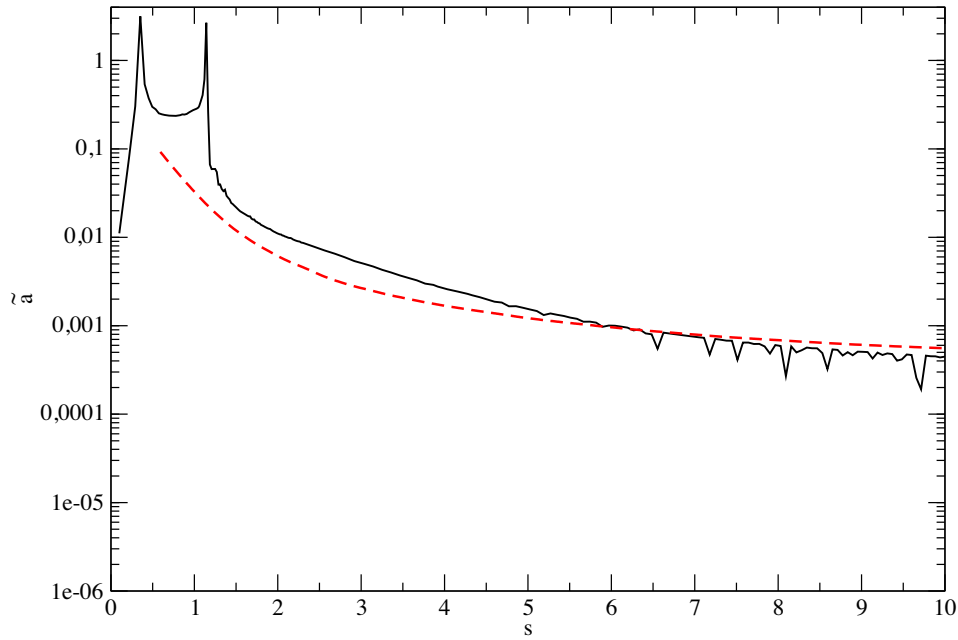


FIG. 9. The evolution of the semimajor axis for the case  $d_0 = 0.95$ . Solid and dashed curves represent the fully numerical result and the result of the solution of (15), respectively.

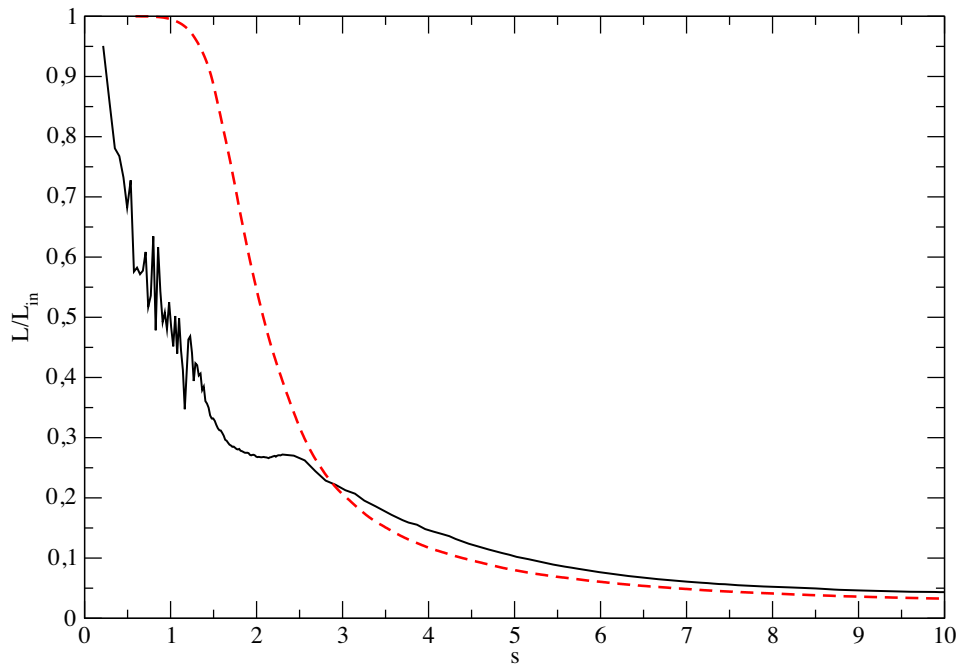


FIG. 10. The same as Fig. 9, but for the evolution of angular momentum.

rate to be in the range  $10 \text{Gpc}^{-3} \text{yr}^{-1} < R < 100 \text{Gpc}^{-3} \text{yr}^{-1}$ , see e.g., Refs. [15,30].

$$t_{\text{GW}} = \frac{3}{170} \frac{c^5}{(GM)^3} a^4 j^7, \quad (16)$$

### A. Timescale of the evolution of semimajor axis

The formation rate  $R$  is determined, to a large extent, by a characteristic timescale of the evolution of  $a$ ,  $t_{\text{GW}}$ , for a bound PBH pair having a large value of initial eccentricity  $e \sim 1$

where  $j = \sqrt{1 - e^2}$ , see e.g., Ref. [30].

The pairs have a time to merge only when  $t_{\text{GW}} < t_H$ , where  $t_H \approx 1.38 \times 10^{10} \text{yr}$  is the present age of the Universe.

We introduce  $\tilde{t}_{\text{GW}} = t_{\text{GW}}/t_H$  and express it in terms of the quantities appropriate for the problem at hand. We obtain

$$\tilde{t}_{\text{GW}} = 5.22 \times 10^{19} j^7 \tilde{a}^4 M_*^{-5/3}, \quad (17)$$

where  $\tilde{a} = a/\bar{R}$  and  $M_* = M/50 M_\odot$ . From the condition  $\tilde{t}_{\text{GW}} < 1$  we obtain

$$\tilde{a} < \tilde{a}_{\text{crit}}, \quad \tilde{a}_{\text{crit}} = 1.17 \times 10^{-5} j^{-7/4} M_*^{5/12}. \quad (18)$$

In what follows we assume that both  $\tilde{a}$  and  $j$  (or, equivalently, the dimensionless angular momentum  $l = \sqrt{\tilde{a}}j$ ) are certain functions of the initial comoving distance  $d_0$ , and a possible form of these functions follow from a particular scenario of the evolution of the pair before the process of its evolution due to emission of gravitational waves sets in. Note that it is different from the approach undertaken by AKK, who considered  $j$  as a stochastic variable, but we are going to show that both approaches give quite similar results in the scenario when the effects of accreting CDM are neglected. When these functions are specified the condition  $t = t_{\text{GW}}$  provide a certain value of  $d_0$  (for given  $f$  and  $M_*$ ),  $d_*(t)$ , and only the pairs with  $d < d_*(t)$  can merge before time  $t$ . When  $t = t_H$  we set  $d_* \equiv d_*(t_H)$ .

Assuming that spatial distribution of PBHs obey the Poisson statistics and introducing the variable  $X = f d_0^3$  instead of  $d_0$ , one can easily show that probability density of distribution over a distance to the closest neighbor having some value of  $X$ ,  $\frac{dP}{dX}$  is  $\frac{dP}{dX} = e^{-X}$ . Accordingly, the probability to have a pair with  $d_0 < d_*$ ,  $P_*$ , is  $\frac{1}{2} X_* e^{-X_*}$ , where the factor  $\frac{1}{2}$  is inserted to avoid double counting of the components, and  $X_* = f d_*^3$ , see also AKK. Taking into account that we expect  $X_* \ll 1$  we can set  $P_* = X_*$ .

In order to estimate the merger rate we need to know the present day number density,  $n_{\text{pbh}}$ . This follows from our definition of the PBH mass fraction  $f$  and the average radius  $\bar{R}$

$$n_{\text{pbh}} = \frac{3f}{4\pi(s_{\text{PT}}\bar{R})^3}, \quad (19)$$

where  $s_{\text{PT}} \approx 5.88 \times 10^3$  is the present day value of the scale factor and we remind the reader that we normalize it by the condition that it is equal to one at the equipartition time. A number density of PBHs, which have been merged before the present time,  $n_{\text{merge}}$ , follows from (19) and the definition of our probability  $P_* = X_*$

$$n_{\text{merge}} = \frac{3}{8\pi} \frac{fX(d_*)}{(s_{\text{PT}}\bar{R})^3}. \quad (20)$$

We obtain the merger rate differentiating  $X$  in (20) and remembering that  $X$  is a function of time due to the

condition  $t = t_{\text{GM}}$  and our assumption that  $\tilde{a}$  and  $j$  entering  $t_{\text{GW}}$  are functions of  $d$ . We have

$$R = \frac{3}{8\pi} \frac{fX(d_*)}{(s_{\text{PT}}\bar{R})^3} \left( \frac{t_{\text{GW}}}{X_*} \frac{\partial X_*}{\partial t_{\text{GW}}} \right) \approx 2.86 \times 10^7 f X_* M_*^{-1} \left( \frac{t_{\text{GW}}}{X_*} \frac{\partial X_*}{\partial t_{\text{GW}}} \right) \text{Gpc}^{-3} \text{yr}^{-1}. \quad (21)$$

## B. The merger rate in case when CDM accretion is neglected

When the influence of accreting CDM on the evolution of semimajor axis and angular momentum of the binary is neglected the problem can be analyzed with the help of solutions to Eq. (5) and calculation of some integrals related to those solutions, see, e.g., AKK, [30]. We closely follow AKK in this paper for an estimate of the event rate in this case and use this estimate as a “reference value” for the problem, which takes into account the effect of clusterization.

When the accretion is neglected one can use  $a_{\text{fin}}$  represented in Fig. 1 as the corresponding value of semimajor axis entering (17). In the same approach  $j$  does change significantly at time  $t > t_{\text{eq}}$  and its value is assumed to be determined by two factors: (1) gravitational torques on the pair from the side of other black holes, and (2) gravitational torques determined by the cosmological density perturbations. In the first case a distribution over possible values  $j$  is given by Eq. (19) of AKK, which can be used to calculate a mean value of  $j$ . However, the corresponding integral is logarithmically divergent, which is related to the fact that nonphysical values of  $j > 1$  are allowed. We set, accordingly, the upper integration limit  $j = 1$  there, thus obtaining the average value

$$j_{\text{bh}} = 0.5f d^3 \Lambda, \quad \Lambda = \ln \frac{4}{f d^3}, \quad (22)$$

where we remind that  $f$  is the ratio of PBH mass density to CDM mass density and it is assumed that  $f \ll 1$ . When  $f \geq 10^{-3}$   $\Lambda \sim 10$ . The average value of  $j$  due to the influence of cosmological perturbations,  $j_{\text{cp}}$  is given by Eq. (21) of AKK. Being rewritten with the help of our notations it has the form

$$j_{\text{cp}} = 2.5 \times 10^{-3} d^3, \quad (23)$$

where we assume that  $\sigma_{\text{eq}} = 5 \times 10^{-3}$  in Eq. (21) of AKK. In order to find a typical value of  $t_{\text{GW}}$  in Eq. (16) we use  $j = j_{\text{bh}}$  when  $j_{\text{bh}} > j_{\text{cp}}$  and  $j = j_{\text{cp}}$  otherwise.

When the result of solution of Eq. (5) and  $j$  given by the expressions above are substituted in (18) the condition  $\tilde{a}_{\text{crit}} = \tilde{a}_{\text{fin}}$  can be used to express  $d_*$  as a function of  $f$ , for a fixed value of  $M_*$ . We show this function in Fig. 11 for the case  $M_* = 1$ . Note that the sawlike behavior of the curve is simply due to relatively small numbers of our grid points



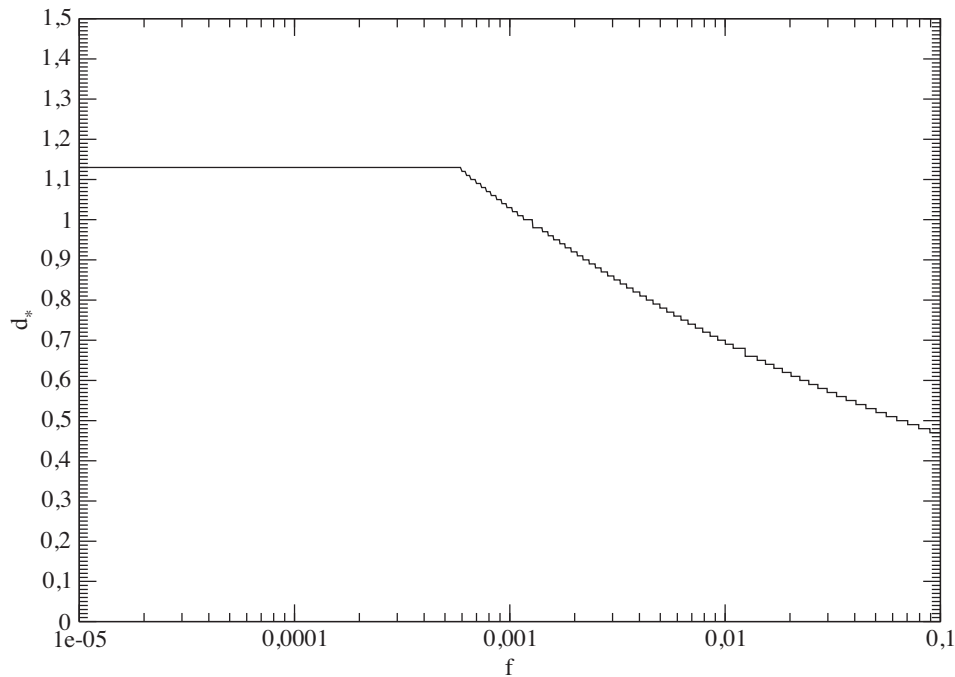


FIG. 11. The quantity  $d_*$  as a function of  $f$  for  $M_* = 1$ .

used to represent our quantity  $d_0$  when solving (5). This is clearly nonphysical, but, since it does not influence any our results it is left unchanged. Also note that  $d_*$  is constant at small values of  $f$ . This is because when  $f$  is small  $j = j_{\text{cp}}$  which does not depend on  $f$ , see Eq. (23).

From Eq. (8) it follows that  $\tilde{a}_{\text{fin}} \propto d_*^4$  when  $d_*$  is not too large, while from the discussion above we see that we may approximate the dependence of  $j$  on  $d_*$  as  $j \propto d_*^3$ . Taking into account that  $X_* = f d_*^3$  we see from Eq. (16) that  $t_{\text{GW}} \propto X_*^{37/3}$  and, accordingly,  $\frac{t_{\text{GW}}}{X_*} \frac{\partial X_*}{\partial t_{\text{GW}}} = \frac{3}{37}$  in (21) when accretion is neglected. We use  $\frac{t_{\text{GW}}}{X_*} \frac{\partial X_*}{\partial t_{\text{GW}}} = \frac{3}{37}$  in Eq. (21), thus obtaining the event rate in the model case of the absence of accretion, which is shown in Fig. 14 below together with an estimate of the event rate, which takes into account the effects of CDM accretion. From this Fig. it is seen that, in the case when accretion is neglected, in order to have  $R$  in the interval  $10 - 100 \text{ Gpc}^{-3} \text{ yr}^{-1}$  the mass fraction  $f$  should be in the interval  $2.5 \times 10^{-3} - 1.2 \times 10^{-2}$ . It agrees perfectly with the corresponding result of AKK [51], see their Fig. 5. From Fig. 11 it also follows that when  $f$  is approximately in the range  $10^{-3} - 10^{-2}$ ,  $d_*$  should approximately be in the range 0.5–1. This justifies the range of  $d_0$  chosen for our numerical simulations.

### C. The merger rate in the case of CDM accretion

#### 1. Numerical evaluation of the quantities of interest and the corresponding fitting procedure

In order to estimate the influence of the CDM accretion on the event rate we performed five simulations with

$d_0 = 0.5, 0.7, 0.95, 1.5,$  and  $2$ . From the expression (16) it follows that  $t_{\text{GW}}$  is determined by the dimensionless angular momentum  $l = \sqrt{\tilde{a}}j$  and  $\tilde{a}$ . Since the estimates (22) and (23) show that the pair is expected to be very eccentric, “realistic” value of initial eccentricity are numerically extremely expensive. Therefore, in order to estimate the evolution of  $l$  we use the following procedure: for each value of  $d_0$  we calculate some initial value of  $l$ ,  $l_{\text{in}}$  during an initial stage of numerical evolution and some final value  $l_{\text{fin}}$  at some final time,  $t_{\text{fin}}$ . Then we calculate the ratio  $\lambda = l_{\text{fin}}/l_{\text{in}}$  and multiply it by  $\sqrt{\tilde{a}_{\text{fin}}j}$ , where  $\tilde{a}_{\text{fin}}$  is determined by the solution of equation (6) and  $j$  is given by (22) or (23), as discussed above. The numerical value of  $\tilde{a}$  used in (16),  $\tilde{a}_{\text{fin}}^{\text{num}}$  is calculated at the same moment of time. This moment of time is taken to correspond to  $s_{\text{fin}} \sim 10$  for the runs with  $d_0 < 1$  and  $s_{\text{fin}} \sim 5$  for the runs with  $d_0 > 1$ , since in the latter case there is no significant evolution of  $\lambda$  and  $\tilde{a}$  further on. We have checked that numerical effects are not expected to influence our results both by performing runs with significantly different values of CDM particles and by comparing the results to the run corresponding to a single black hole. It is important to stress that the procedure of evaluation of the final angular momentum explicitly implies the assumption that torques acting on the pair are proportional to its angular momentum. Although it is supported by theory when binary evolves in the hardening regime, see Eq. (14), and finds some evidences in our numerical simulations, since the runs corresponding to  $d_0 = 0.5$  have much smaller initial values of angular momentum, see Fig. 6, a caution should

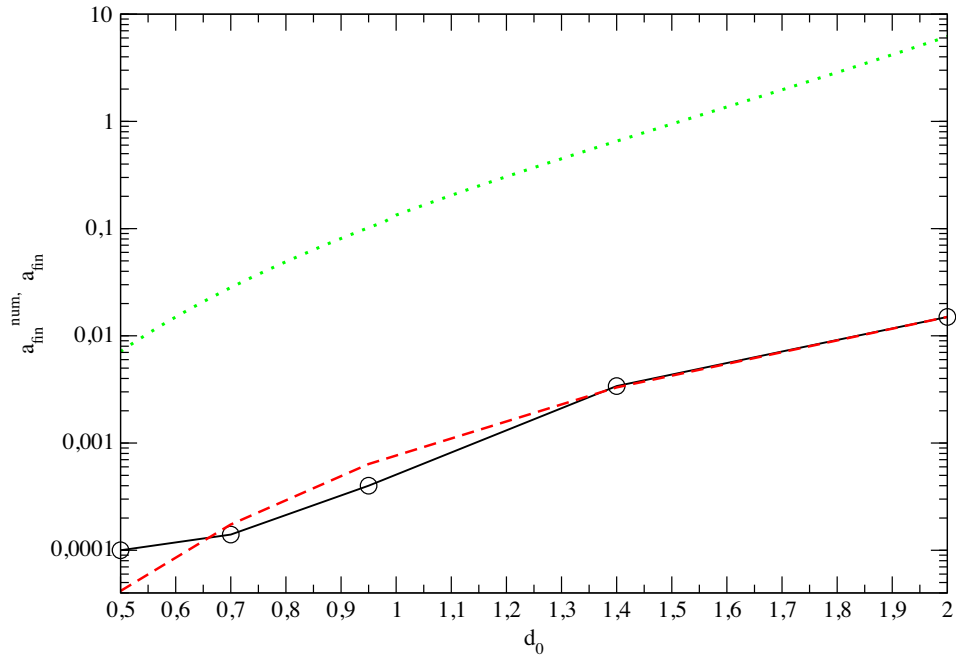


FIG. 12. We show the values of  $\tilde{a}_{\text{fin}}^{\text{num}}$  as the solid line, a power law fit of the numerical results by the dashed line and the result of the solution of (6) as the dotted line. Symbols corresponds to the values obtained in the different numerical runs with different values of  $d_0$ .

be taken with respect to this point. We are going to check this assumption with special purpose simulations in our future work.

We show  $\tilde{a}_{\text{fin}}^{\text{num}}$  and  $\lambda$  in Figs. 12 and 13. As seen from Fig. 12 the numerically obtained values of  $\tilde{a}_{\text{fin}}$  are roughly

two orders of magnitude smaller than the analytical ones. However, the slopes of the numerical and analytical curves are similar. The dashed curve shows the power law fit

$$\tilde{a}_{\text{fin}}^{\text{num}} = 7.9 \times 10^{-4} d^{4.24}, \quad (24)$$

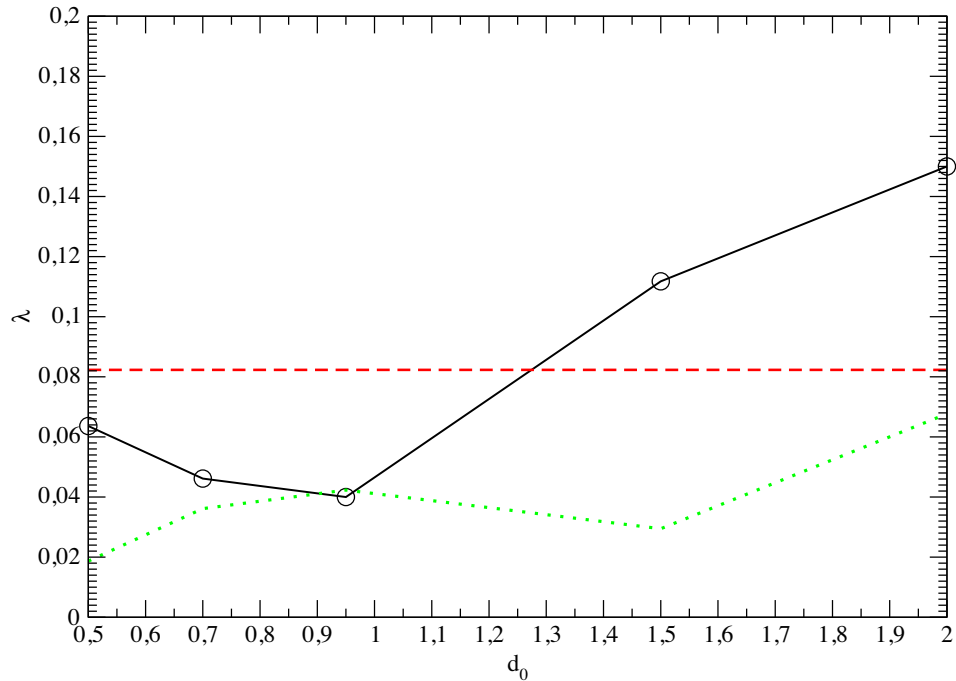


FIG. 13. The dependency of the quantity  $\lambda$  on  $d_0$  is shown. As in the previous figure solid line and symbols correspond to the numerical results. The dashed line show the average value of  $\lambda$ ,  $\lambda_{\text{av}}$  and the dotted line shows the deviation  $|\lambda - \lambda_{\text{av}}|$ .

which gives an excellent agreement with the data apart from the case with the smallest  $d_0 = 0.5$ , where it disagrees by factor of two.

In Fig. 13 we show the dependency of  $\lambda$ . One can see that  $\lambda$  depends nonmonotonically on  $d_0$ . However, its average value,  $\lambda_{av} = 8.23 \times 10^{-2}$  approximates the data points with the accuracy order of or less than 50 percent for all runs.

## 2. An estimate of the merger rate

Given the complexity of the problem on hand we can consider an evaluation of the merger event rate based on the numerical results as a preliminary estimate. Since from Fig. 1 it follows that we can use the analytic expression for  $a_{\text{fin}}$  given by Eq. (8) for a qualitative estimates when  $d_0 < 0$ , we are going to use (24) and  $\lambda_{av}$  and all other ingredients needed for the estimate are simple functions of the parameters of the problem, we can make it analytically. For that we proceed as follows.

At first, from Eqs. (8), (22) and (23) it is seen that the dimensionless value of angular momentum after the accretion stage can be estimated as

$$l_{\text{fin}} = \lambda_{av} j_{\text{bh}} \sqrt{\tilde{a}_{\text{fin}}} \approx 1.32 \times 10^{-2} f d^5 \Lambda, \quad (25)$$

in case when  $f > f_{\text{crit}}$  and

$$l_{\text{fin}} = \lambda_{av} j_{\text{cp}} \sqrt{\tilde{a}_{\text{fin}}} \approx 6.47 \times 10^{-5} d^5, \quad (26)$$

in the opposite case, while from the data represented in Fig. 11 it follows that  $f_{\text{crit}} \approx 6 \times 10^{-4}$ . Next, we express (17) in terms of  $l_{\text{fin}}$  and  $\tilde{a}_{\text{fin}}^{\text{num}}$  as

$$\tilde{t}_{\text{GW}} = 5.22 \times 10^{19} l_{\text{fin}}^7 \sqrt{(\tilde{a}_{\text{fin}}^{\text{num}})} M_*^{-5/3}. \quad (27)$$

Now we can substitute (24), (25), and (26) into (27) and, using the condition  $\tilde{t}_{\text{GW}} = 1$  obtain a value of  $d_0$ ,  $d_*$ , corresponding to the pairs, which are merging at the present time.

We have

$$d_* = 0.735 \cdot (\Lambda f)^{-0.188} M_*^{0.048} \quad (28)$$

when  $f > f_{\text{crit}}$  and

$$d_* = 2M_*^{0.048}. \quad (29)$$

Note that Eq. (28) give, strictly speaking, an implicit expression for  $d_*$ , since  $\Lambda$  depends on  $d_*$  itself, see Eq. (22). However, it is also seen that the dependency of  $\Lambda$  in (28) is quite weak, and  $\Lambda$  depends on  $d_*$  logarithmically. Therefore, for our estimate below we are going to set  $d = 1$  in (22) and use  $\Lambda = \ln \frac{4}{f}$ . Also note that from Eqs. (28) and (29) it follows that  $d_*$  is expected to be order of unity.

Since the dependency of  $t_{\text{GW}}$  on  $d$  is close to the case of no accretion, we are going again to use  $\frac{t_{\text{GW}}}{X_*} \frac{\partial X_*}{\partial t_{\text{GW}}} = \frac{3}{37}$  in (21), thus obtaining

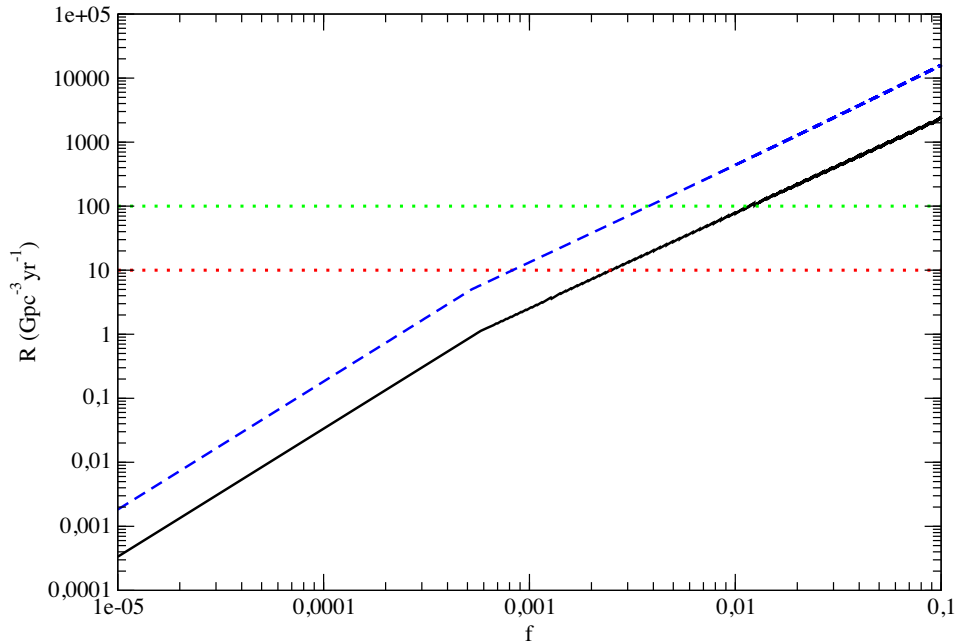


FIG. 14. The merger rate as a function of PBH mass fraction  $f$  for  $M_* = 1$ . The solid curve shows the rate obtained under the assumption that CDM accretion effects are negligible, the dashed line shows our estimate given by Eqs. (31) and (32), which takes into account the effects of accretion. The horizontal dotted lines show the values  $R = 10$  and  $100$  assumed to be the margins provided by observations.

$$R = 2.13 \times 10^6 f^2 d_*^3 M_*^{-1} \text{ Gpc}^{-3} \text{ yr}^{-1}. \quad (30)$$

We substitute (28) and (29) in (30) and obtain

$$R = 0.91 \times 10^6 f^{1.44} \Lambda^{-0.564} M_*^{-0.856} \text{ Gpc}^{-3} \text{ yr}^{-1} \quad (31)$$

and

$$R = 1.82 \times 10^7 f^2 M_*^{-0.856} \text{ Gpc}^{-3} \text{ yr}^{-1}, \quad (32)$$

for the cases  $f > f_{\text{crit}}$  and  $f < f_{\text{crit}}$ , respectively.

We show results of evaluation of the event rate in Fig. 14. The case when accretion is neglected is shown as solid line, while the case when the effects of accretion are accounted for is represented by dashed line. From this figure it is seen that both cases have approximately the same dependency on  $f$ , but the latter estimate gives values of  $R$  larger than the ones given by the former, in approximately 6–8 times. Therefore, in order to satisfy the observational limits on the merger rate,  $f$  should be smaller in the case when the effects of accretion are taken into account. Namely, in this case it should be in the range  $7.5 \times 10^{-4} - 3.4 \times 10^{-3}$  contrary to the standard case when the corresponding range is  $2.5 \times 10^{-3} - 1.2 \times 10^{-2}$ .

## V. CONCLUSIONS AND DISCUSSION

In this paper we consider the influence of interaction of CDM particles with pairs of PBHs immersed in a medium consisting of radiation and CDM experiencing the standard cosmological expansion. The pairs become bound at times comparable to the equipartition time,  $t_{\text{eq}}$ , when both CDM and radiation matter densities are equal to  $\rho_{\text{eq}}$ . We run simulations with a direct summation N-body code and find numerically that a halo of CDM particles having small angular momenta is formed around the pair after it has become bound, with mass  $M_{\text{halo}}$  growing approximately proportional to the scale factor,  $M_{\text{halo}} \propto s$ , and the density distribution following the power law  $\rho \propto r^{-9/4}$ , confirming earlier analytical predictions. The density distribution is almost stationary at times  $t \geq t_{\text{eq}}$ . Before the formation of the bound pair, provided that the initial comoving separation is large enough, two separate massive halos are formed around two black holes. These halos are then destructed during the formation time of the bound pair. We call the bound pairs as “binary PBHs” and consider values of their parameters (the mass  $M = 50 M_{\odot}$  and initial comoving separations,  $d_0$ , expressed in unit of the radius  $\bar{R} = (\frac{3M}{4\pi\rho_{\text{eq}}})^{1/3}$ ), which are of interest for the problem of the formation of the sources of gravitational waves due to merger of PBH pairs at the present time, possibly explaining the LIGO events. The initial mass fraction of PBHs,  $f$ , is assumed to be small.

Since the angular momentum of CDM particles residing in the halos is low, they can come close to the binary and

gravitationally interact with it in an efficient way, causing an exchange of energy and angular momentum between the particles and the binary. It is found numerically, that, as a result of these interactions the binary PBH significantly reduce values of its semimajor axis and angular momentum of the binary. We calculate the evolution of semimajor and angular momentum, taking also into account tidal field caused by the presence of radiation matter density. The radiation is assumed to be unclustered and its matter density obeys the standard cosmological evolution law. Our calculations are started at the epoch of radiation dominated and ended sufficiently deep into the matter-dominated stage.

We consider several values of  $d_0$  in the range 0.5–2 and a value of the scale factor corresponding to the end time of our calculations, typically ten times larger than that corresponds to  $t_{\text{eq}}$ . We find that, at the end time of our calculations, the binary angular momentum is typically ten times smaller than its initial value, while a value of semimajor axis is typically one hundred times smaller than the one obtained in the calculations, which do not take into account the effect of CDM clustering. Physical origin of these changes seems, however, appears to be different for the binaries having  $d_0 > 1$  and  $d_0 < 1$ . In the former case it is mainly caused by strong nonstationary processes occurring during the formation time of the bound pair. During this time a large value of mass of CDM particles is expelled from the system, causing rather abrupt changes of semimajor axis and angular momentum. In the latter case the evolution mainly proceeds in a secular way, and may be explained by the process of hardening of the binary due to the interaction with CDM particles. We provide a semi-analytical treatment of this process, which is in an excellent agreement with the numerical results at late times.

The reason why purely analytical methods appear to be difficult to implement for the problem on hand is because of relatively rather large values of angular momentum of the halo’s particles. In our setting of the problem the only physical origin of the angular momentum is provided by torques acting on the particles from the side of quadruple component of the gravitational field of the pair. We have checked, however, that these torques alone cannot produce values of angular momentum observed in the simulations. On the other hand, we have checked that these values cannot be explained by numerical effects, using simulations with a different total number of low mass particles, representing CDM, and comparing results of the simulations of a pair with an auxiliary simulation having a single PBH of doubled mass. We propose the following qualitative picture for an explanation of this issue. The torques provided by the pair excite nonaxisymmetric perturbations of matter density of CDM particles. These perturbations are amplified in the halo as a results of various potential instabilities, e.g., the instability of radial orbits, see, e.g., Ref. [50]. The gravitational field associated with the amplified perturbations causes the torque large enough

to explain the obtained values of angular momentum. Clearly, this picture requires a further detailed analysis.

We use the values of angular momentum and semimajor axis obtained at the end time of our simulations to demonstrate to what extent the effects considered in this paper could influence the merger rate. For that, at first, we simplify the approach developed in [30] in a way, which can be directly used in both case when the CDM clustering is neglected (the standard case) and when it is taken into account. We show, that, regardless of these simplifications, our way to estimate the merger rate quantitatively reproduces the results reported in [30] in the case of no clustering. In the case when the clustering is considered the merger rate is shown to be 6–8 times larger than in the standard case. This, in turn, means that values of  $f$  needed to satisfy the observational limits on the merger rate are several times smaller than in the standard case. We also provide a simple analytical expressions for the merger rate, which can be directly used in case of a distributed mass spectrum of PBHs.

Our results should be considered as preliminary ones. For example, the process of hardening does not stop at the end time of our simulation. It could, potentially, operate up to much later times, thus further decreasing semimajor axis and angular momentum. This, would, obviously, mean even larger values of the merger rate at a fixed value of  $f$ . A physically motivated end time of this process may, in principle, be the time of a significantly nonlinear structure

formation at the scales of interest, corresponding to redshifts order of ten. On the other hand, halo may become more perturbed at late times due to a slow growth of various instabilities and input of the factors neglected in this work (e.g., the influence of other PBHs, development of the halo’s perturbations seeded by the cosmological ones). These processes may quench binary’s hardening at late times. Another interesting development is associated with the process of accretion of baryonic matter, which may be significant at redshifts order of ten, see, e.g., Refs. [52,53]. This process may also contribute to an additional significant change of the orbital parameters of the binary, see [54] for analytic estimates of the significance of this process. All these issues as well as the issue of relatively large angular momenta of the halo’s particles are left for a potential future work.

Finally, we note that simulating PBH pairs with CDM to much larger times is a numerical challenge. Direct summation methods are too slow, while approximate methods, like a tree algorithm used in `Gadget-2` or `Gadget-4` code do not provide good enough accuracy, according to our tests.

## ACKNOWLEDGMENTS

This work was supported in part by RFBR Grant No. 19-02-00199. We are grateful to Maxim Pshirkov for very useful comments.

- 
- [1] S. Hawking, Gravitationally collapsed objects of very low mass, *Mon. Not. R. Astron. Soc.* **152**, 75 (1971).
  - [2] B. C. Lacki and J. F. Beacom, Primordial black holes as dark matter: Almost all or almost nothing, *Astrophys. J. Lett.* **720**, L67 (2010).
  - [3] K. M. Belotsky, A. E. Dmitriev, E. A. Esipova, V. A. Gani, A. V. Grobov, M. Y. Khlopov, A. A. Kirillov, S. G. Rubin, and I. V. Svadkovsky, Signatures of primordial black hole dark matter, *Mod. Phys. Lett. A* **29**, 1440005 (2014).
  - [4] A. Kashlinsky, LIGO gravitational wave detection, primordial black holes, and the near-IR cosmic infrared background anisotropies, *Astrophys. J. Lett.* **823**, L25 (2016).
  - [5] S. Clesse and J. Garca-Bellido, The clustering of massive primordial black holes as dark matter: Measuring their mass distribution with Advanced LIGO, *Phys. Dark Universe* **15**, 142 (2017).
  - [6] S. Clesse and J. Garca-Bellido, Seven hints for primordial black hole dark matter, *Phys. Dark Universe* **22**, 137 (2018).
  - [7] J. R. Espinosa, D. Racco, and A. Riotto, Cosmological Signature of the Standard Model Higgs Vacuum Instability: Primordial Black Holes as Dark Matter, *Phys. Rev. Lett.* **120**, 121301 (2018).
  - [8] B. J. Carr and M. J. Rees, Can pregalactic objects generate galaxies?, *Mon. Not. R. Astron. Soc.* **206**, 801 (1984).
  - [9] R. Bean and J. a. Magueijo, Could supermassive black holes be quintessential primordial black holes?, *Phys. Rev. D* **66**, 063505 (2002).
  - [10] B. Carr and F. Kühnel, Primordial black holes as dark matter: Recent developments, *Annu. Rev. Nucl. Part. Sci.* **70**, 355 (2020).
  - [11] B. Carr and F. Kühnel, Primordial black holes as dark matter candidates, *SciPost Phys. Lect. Notes* **48**, 1 (2022).
  - [12] A. G. Polnarev and M. Yu. Khlopov, Cosmology, primordial black holes and supermassive particles, *Soviet Physics Uspekhi* **28**, 213 (1985).
  - [13] B. P. Abbott, R. Abbott, T. D. Abbott, M. R. Abernathy, F. Acernese, K. Ackley, C. Adams, T. Adams, P. Addesso, and R. X. Adhikari, Observation of Gravitational Waves from a Binary Black Hole Merger, *Phys. Rev. Lett.* **116**, 061102 (2016).
  - [14] B. P. Abbott, R. Abbott, T. D. Abbott, M. R. Abernathy, F. Acernese, K. Ackley, C. Adams, T. Adams, P. Addesso, and R. X. Adhikari, GW151226: Observation of Gravitational Waves from a 22-Solar-Mass Binary Black Hole Coalescence, *Phys. Rev. Lett.* **116**, 241103 (2016).



- [15] B. P. Abbott, R. Abbott, T. D. Abbott, M. R. Abernathy, F. Acernese, K. Ackley, C. Adams, T. Adams, P. Addesso, and R. X. Adhikari, Astrophysical implications of the binary black-hole merger GW150914, *Astrophys. J. Lett.* **818**, L22 (2016).
- [16] B. P. Abbott, R. Abbott, T. D. Abbott, F. Acernese, K. Ackley, C. Adams, T. Adams, P. Addesso, R. X. Adhikari, and V. B. Adya, GW170104: Observation of a 50-Solar-Mass Binary Black Hole Coalescence at Redshift 0.2, *Phys. Rev. Lett.* **118**, 221101 (2017).
- [17] B. P. Abbott, R. Abbott, T. D. Abbott, F. Acernese, K. Ackley, C. Adams, T. Adams, P. Addesso, R. X. Adhikari, and V. B. Adya, GW170814: A Three-Detector Observation of Gravitational Waves from a Binary Black Hole Coalescence, *Phys. Rev. Lett.* **119**, 141101 (2017).
- [18] B. P. Abbott, R. Abbott, T. D. Abbott, F. Acernese, K. Ackley, C. Adams, T. Adams, P. Addesso, R. X. Adhikari, and V. B. Adya, GW170608: Observation of a 19 solar-mass binary black hole coalescence, *Astrophys. J. Lett.* **851**, L35 (2017).
- [19] B. P. Abbott, R. Abbott, T. D. Abbott, F. Acernese, K. Ackley, C. Adams, T. Adams, P. Addesso, R. X. Adhikari, and V. B. Adya, Properties and astrophysical implications of the  $150 M_{\odot}$  binary black hole merger GW190521, *Astrophys. J. Lett.* **900**, L13 (2020).
- [20] LIGO/Virgo Public Alerts from the O3/2019 observational run can be found at <https://gracedb.ligo.org/superevents/public/O3/>.
- [21] E. D. Kovetz, Probing Primordial Black Hole Dark Matter with Gravitational Waves, *Phys. Rev. Lett.* **119**, 131301 (2017).
- [22] M. Sasaki, T. Suyama, T. Tanaka, and S. Yokoyama, Primordial Black Hole Scenario for the Gravitational-Wave Event GW150914, *Phys. Rev. Lett.* **117**, 061101 (2016).
- [23] S. Blinnikov, A. Dolgov, N. K. Porayko, and K. Postnov, Solving puzzles of GW150914 by primordial black holes, *J. Cosmol. Astropart. Phys.* **11** (2016) 036.
- [24] Note, however, that some of the LIGO events may have another origin, see, e.g., Ref. [25]. It is important to stress that even if all LIGO events will be shown to be due to mergers of black holes of stellar origin, it would give a very nontrivial constraint on the abundance of PBHs of stellar masses in the Universe provided there is a reliable way of an estimate of the formation of PBHs pairs with orbital parameters appropriate for the LIGO events for a given abundance of PBH. The exact possible mass fraction of PBHs in dark matter (DM) in LIGO mass range is still a subject of large theoretical uncertainties, see, e.g., Refs. [26,27].
- [25] A. H. Nitz, C. Capano, A. B. Nielsen, S. Reyes, R. White, D. A. Brown, and B. Krishnan, 1-OGC: The first open gravitational-wave catalog of binary mergers from analysis of public Advanced LIGO data, *Astrophys. J.* **872**, 195 (2019).
- [26] M. Zumalacárregui and U. c. v. Seljak, Limits on Stellar-Mass Compact Objects as Dark Matter from Gravitational Lensing of Type Ia Supernovae, *Phys. Rev. Lett.* **121**, 141101 (2018).
- [27] J. Garcia-Bellido, S. Clesse, and P. Fleury, LIGO Lo(g) Normal MACHO: Primordial black holes survive SN lensing constraints, *Phys. Dark Universe* **20**, 95 (2018).
- [28] S. Mukherjee and J. Silk, Can we distinguish astrophysical from primordial black holes via the stochastic gravitational wave background?, *Mon. Not. R. Astron. Soc.* **506**, 3977 (2021).
- [29] T. Nakamura, M. Sasaki, T. Tanaka, and K. S. Thorne, Gravitational waves from coalescing black hole MACHO binaries, *Astrophys. J.* **487**, L139 (1997).
- [30] Y. Ali-Haïmoud, E. D. Kovetz, and M. Kamionkowski, Merger rate of primordial black-hole binaries, *Phys. Rev. D* **96**, 123523 (2017).
- [31] Among the alternative scenarios let us mention the scenario of the formation of the bound pairs in galactic cusps at relatively late time, see, e.g., Refs. [32,33]. Note, however, that this scenario seems to require a large mass fraction of PBHs  $f \sim 1$ , which may be refuted by the constraints on  $f$  in this mass range, see, e.g., Ref. [34].
- [32] S. Bird, I. Cholis, J. B. Muñoz, Y. Ali-Haïmoud, M. Kamionkowski, E. D. Kovetz, A. Raccanelli, and A. G. Riess, Did LIGO Detect Dark Matter?, *Phys. Rev. Lett.* **116**, 201301 (2016).
- [33] S. Fakhry, J. T. Firouzjaee, and M. Farhoudi, Primordial black hole merger rate in ellipsoidal-collapse dark matter halo models, *Phys. Rev. D* **103**, 123014 (2021).
- [34] B. Carr, K. Kohri, Y. Sendouda, and J. Yokoyama, Constraints on primordial black holes, *Rep. Prog. Phys.* **84**, 116902 (2021).
- [35] K. J. Mack, J. P. Ostriker, and M. Ricotti, Growth of structure seeded by primordial black holes, *Astrophys. J.* **665**, 1277 (2007).
- [36] Y. N. Eroshenko, Dark matter density spikes around primordial black holes, *Astron. Lett.* **42**, 347 (2016).
- [37] B. J. Kavanagh, D. Gaggero, and G. Bertone, Merger rate of a subdominant population of primordial black holes, *Phys. Rev. D* **98**, 023536 (2018).
- [38] By a binary PBH we understand later on a gravitationally bound pair of PBHs. We use both these terms interchangeably below.
- [39] Note that the energy is not conserved initially, when tidal forces determined by expansion of the Universe dominate over gravity of the binary. Nonetheless, we use the usual Keplerian definitions of binding energy and semimajor axis at all times.
- [40] D. C. Hogg, Binary evolution in stellar dynamics, *Mon. Not. R. Astron. Soc.* **173**, 729 (1975).
- [41] Note that one can also, in principle, include the dynamic friction term in this equation. However, it can be shown to be small during the radiation dominated stage due to the effect discussed in [42].
- [42] G. S. Bisnovaty-Kogan and I. G. Shukhman, Particle collisions in an expanding universe, *Zh. Eksp. Teor. Fiz.* **82**, 3 (1982).
- [43] S. Portegies Zwart *et al.*, A multiphysics and multiscale software environment for modeling astrophysical systems, *New Astron.* **14**, 369 (2009).
- [44] A. van Elteren, I. Pelupessy, and S. P. Zwart, Multi-scale and multi-domain computational astrophysics, *Phil. Trans. R. Soc. A* **372**, 20130385 (2014).
- [45] J. R. Gott, On the formation of elliptical galaxies, *Ap. J.* **201**, 296 (1975).
- [46] J. E. Gunn, Massive galactic halos. I. Formation and evolution, *Astrophys. J.* **218**, 592 (1977).

- [47] E. Bertschinger, Self-similar secondary infall and accretion in an Einstein-de Sitter universe, *Astrophys. J. Suppl. Ser.* **58**, 39 (1985).
- [48] Note that this result is different from that obtained in [35], who claimed that  $\rho \propto r^{-3}$ .
- [49] A. Sesana, F. Haardt, and P. Madau, Interaction of massive black hole binaries with their stellar environment. I. Ejection of hypervelocity stars, *Astrophys. J.* **651**, 392 (2006).
- [50] E. V. Polyachenko and I. G. Shukhman, Radial orbit instability in systems of highly eccentric orbits: Antonov problem reviewed, *Mon. Not. R. Astron. Soc.* **470**, 2190 (2017).
- [51] Note that the value of  $M_*$  in their Fig. 5, which is the closest to our value  $M_* = 1$ , is  $M_* = 3/5$ . This shouldn't, however, influence the agreement in any significant way.
- [52] V. De Luca, G. Franciolini, P. Pani, and A. Riotto, Constraints on primordial black holes: The importance of accretion, *Phys. Rev. D* **102**, 043505 (2020).
- [53] G. Hasinger, Illuminating the dark ages: Cosmic backgrounds from accretion onto primordial black hole dark matter, *J. Cosmol. Astropart. Phys.* **07** (2020) 022.
- [54] V. De Luca, G. Franciolini, P. Pani, and A. Riotto., Primordial Black Holes confront LIGO/VIRGO data: Current situation, *J. Cosmol. Astropart. Phys.* **06** 044 (2020).